Research Square

Preprints are preliminary reports that have not undergone peer review.
They should not be considered conclusive, used to inform clinical practice,
or referenced by the media as validated information.

Targeting LL-37-Driven Psoriasiform Inflammation with Apolipoprotein A-I

Joanna Koziel

joanna.koziel@uj.edu.pl

Jagiellonian University https://orcid.org/0000-0003-3436-6425

Anna Golda

Jagiellonian University

Alicia Wong

Jagiellonian University

Dominik Kowalczyk

Jagiellonian University

Karina Adamowicz

Jagiellonian University

Danuta Bryzek

Jagiellonian University

Dorota Satala

Jagiellonian University

Firdaus Samsudin

Bioinformatics Institute (BII), Agency for Science, Technology and Research (A*STAR)

Peter Bond

Bioinformatics Institute (BII), Agency for Science, Technology and Research (A*STAR)

Maria Rapala-Kozik

Jagiellonian University

Jan Potempa

Department of Oral Immunology and Infectious Diseases, School of Dentistry, University of Louisville
https://orcid.org/0000-0002-3600-7461

Artur Schmidtchen

Division of Dermatology https://orcid.org/0000-0001-9209-3141

Article

Keywords:

Posted Date: November 19th, 2026

DOI: https://doi.org/10.21203/rs.3.rs-11783966/v1

License: This work is licensed under a Creative Commons Attribution 4.0 International License.
Read Full License

Additional Declarations: There is **NO** Competing Interest.

Abstract

Psoriasis is a chronic inflammatory skin disease characterized by dysregulated innate and adaptive immune responses. The antimicrobial peptide LL-37 is increased in psoriatic skin and can promote inflammation through effects on cellular damage, leukocyte recruitment, cytokine production, and the formation of immunostimulatory complexes with self-derived nucleic acids. Here, we investigated whether the human plasma protein apolipoprotein A-I (ApoA-I) can regulate LL-37 activity and thereby attenuate psoriasis-associated inflammation. We show that ApoA-I acts as a scavenger of LL-37 and that its administration confers therapeutic benefits in psoriatic skin, as demonstrated in an experimental animal model and human ex vivo models. Mechanistically, ApoA-I limited nucleic acid uptake and TLR-dependent type I interferon responses in plasmacytoid dendritic cells and keratinocytes. In an experimental mouse model, ApoA-I attenuated imiquimod-induced psoriasiform inflammation, reducing clinical, histological, and molecular disease features, while also suppressing inflammatory mediators and psoriasis-associated biomarkers in a human 3D psoriatic skin model. Together, these findings identify ApoA-I as a previously unrecognized regulator of LL-37-driven skin inflammation and suggest that therapeutic strategies aimed at restoring or mimicking ApoA1´s LL-37-scavenging mechanisms may have potential for treatment of psoriasis and related inflammatory skin diseases.

Introduction

LL-37 is classified as one of the crucial host defense peptides in humans. It possesses strong antimicrobial activity due to its amphipathic and cationic character. The peptide kills microorganisms by permeabilizing their cell membrane but also neutralizes bacterial lipopolysaccharide (LPS)[1–3]. Despite its protective and beneficial role in host defense, LL-37 can act as a potent pro-inflammatory mediator when overexpressed and secreted at high concentrations. It has been shown that elevated LL-37 levels reduce host cells viability and promote apoptosis of osteoblasts, smooth muscle cells, periodontal ligament cells, T cells and neutrophils[4–8]. LL-37-mediated permeabilization of host cells leads to the release of damage associated molecular patterns (DAMPs), including alarmins such as ATP, DNA, histone, high-mobility group protein-1 (HMGB1)[9]. In addition, LL-37 functions as a chemoattractant for neutrophils and eosinophils via the formyl-peptide receptor (FPR)[10] and activates neutrophils, monocytes, and T cells through formyl-peptide receptor like 1 (FPRL1)[11]. Another notable feature of LL-37 is its ability to promote type I IFNs expression by binding nucleic acids and enhancing their recognition by TLR 9 and TLR 7[12]. Furthermore, LL-37 associated with neutrophils and neutrophil extracellular traps (NETs) can be recognized by autoantibodies, accelerating NETs formation and promoting the accumulation of LL-37:DNA complexes[13]. These pro-inflammatory activities of LL-37 have been implicated in the development of autoimmune diseases[14], including rheumatoid arthritis (RA)[15, 16], rosacea[17, 18], systemic lupus erythematosus (SLE)[12, 13, 19], and psoriasis[12, 20–22].

Psoriasis is a common, chronic, immune-mediated inflammatory skin disease with a multifactorial pathogenesis. Although modern targeted therapies have substantially improved disease control, many

patients require long-term treatment, and psoriasis remains a major global health burden affecting more than 100 million individuals worldwide[23]. Patients with psoriasis are at increased risk of developing serious comorbidities, including psoriatic arthritis, cardiovascular disorders, and other conditions such as anxiety and depression, non-alcoholic fatty liver disease, Crohn's disease, and lymphoma[24–26]. The choice of psoriasis treatment depends on disease severity. Mild cases are typically managed with topical therapies, including glucocorticosteroids or vitamin D analogues, whereas moderate to severe psoriasis requires systemic treatment, including biologic therapies targeting tumor necrosis factor-α (TNF-α), interleukin-17 (IL-17), and interleukin-23 (IL-23)[24, 27, 28]. However, a major limitation of these therapies is the long-term immunosuppression, which may increase the risk of infections and malignancies[27, 28]. Therefore, there remains a continuous need to develop novel therapeutic strategies for the treatment of psoriasis. In this context, LL-37 represents a promising therapeutic target, as its concentration in psoriatic skin is estimated to reach up to 304 μM[12] and it promotes self-perpetuating inflammation that is detrimental to the host.

Several congenital mechanisms have been described that restrain excessive expression and/or activity of LL-37. These include proteolytic degradation by enzymes such as neutrophil elastase and cathepsin D, which generate truncated LL-37 peptides with altered inflammatory properties compared with the native peptide[29]. In addition, citrullination/deimination of LL-37 catalyzed by peptidylarginine deiminase abolishes its ability to bind DNA, thereby impairing its pro-inflammatory functions[30]. There have been several attempts to counteract elevated levels of LL-37 using compounds that preserve its antibacterial and anti-endotoxin properties while simultaneously reducing its pro-inflammatory activity. These include heparin and glycosaminoglycans (GAGs), which form complexes with LL-37 and thereby reduce its cationic charge[31]. Another approach involves the use of small inhibitors, such as suramin, which limit the interaction of LL-37 with phospholipid membranes[32]. However, there is a lack of data confirming the clinical effectiveness of such applications.

In psoriasis, LL-37 forms complexes with self-DNA released from damaged cells, promoting plasmacytoid dendritic cell activation and type I interferon production, a mechanism considered central to disease initiation and amplification[20, 21]. Given the known ability of apolipoprotein A-I (ApoA-I), an abundant plasma protein involved in reverse cholesterol transport[33], to bind LL-37 in a noncovalent manner[34] we investigated whether ApoA-I can function as a natural LL-37 scavenger and thereby limit LL-37-associated pro-inflammatory activity in psoriasis.

Here, we demonstrate that ApoA-I neutralizes the pro-inflammatory activity of LL-37, leading to the dissociation of LL-37:nucleic acid complexes and restricting the activation of stromal and epithelial cells, as well as the interferon response in skin-resident cells. In this way, it limits the release of chemokines and the subsequent infiltration of neutrophils, as demonstrated in the imiquimod-induced (IMQ) model of psoriasis. Collectively, these findings reveal a previously unrecognized role for ApoA-I in regulating LL-37 activity and provide a basis for the development of potential novel treatments for autoimmune and inflammatory diseases associated with the accumulation of LL-37.

Materials and Methods

Reagents

Cell culture media and supplements were purchased from Gibco (Thermo Fisher Scientific). Cell culture plasticware was obtained from TPP (Trasadingen). Human blood for peripheral blood mononuclear cell (PBMC) isolation was provided by the Red Cross (Kraków, Poland). Blood samples were deidentified by the provider to ensure donor confidentiality; therefore, the study was exempt from human subjects research approval. CpG oligodeoxynucleotides (ODN 2216) with a phosphorothioate backbone (5'-ggGGGACGATCGTCgggggg-3') were synthesized by InvivoGen (San Diego, CA, USA). Native LL-37, CRAMP and scrambled LL-37 (sLL-37) peptides were synthesized as previously described[35]. Apolipoprotein A-I (ApoA-I), apolipoprotein E (ApoE), and calcipotriol were purchased from Sigma-Aldrich.

Protein-protein docking

To model the binding of LL-37 peptide to ApoA-I, we performed protein-protein docking using the ClusPro webserver[36]. The crystal structure of a truncated human ApoA-I tetramer was obtained from the Protein DataBank (PDB: 1AV1)[37]. The structure of the LL-37 peptide was generated using the AlphaFold webserver[38]. The top ranked model of LL-37 from AlphaFold was docked to the crystal structure of ApoA-I monomer using ClusPro default settings and 10 models (model 0 to 9) were generated for subsequent atomistic molecular dynamics (MD) simulations.

Atomistic molecular dynamics simulations

The binding stability of ClusPro-derived ApoA-I:LL37 complex models was tested using all-atom MD simulations. For each of the 10 generated models, the protein complex was parameterized using the CHARMM36m forcefield[39] and placed inside a 15 nm × 15 nm × 15 nm cubic box. The system was solvated with TIP3P water molecules and neutralized with 0.15 M NaCl. Steepest descent energy minimization was conducted to remove any inter-atomic clashes, followed by short 1-ns NVT and NPT equilibration simulations, whereby the backbone atoms of the proteins were positionally restrained using a force constant of 1,000 kJ mol^{-1} nm^{-1}. Three independent 200 ns production simulations were run for each model using different initial velocity distributions. The Nosé–Hoover thermostat was used to maintain the temperature of the system at 310 K[40, 41]. The Parrinello-Rahman barostat was isotropically coupled to the system to maintain a pressure of 1 atm[42]. Electrostatic interactions were computed using the smooth particle mesh Ewald (PME) method[43], while the van der Waals interactions were truncated at 1.2 nm with a force-switch smoothing function applied between 1-1.2 nm. All covalent bonds with hydrogens were constrained using the LINCS algorithm[44]. Simulations were performed using GROMACS 2025[45] and visualized using VMD[46]. Contact analysis, root mean square deviation (RMSD) measurement,

and Molecular Mechanics Poisson–Boltzmann Surface Area (MM/PBSA) binding free energy calculations were conducted using GROMACS.

Bio-layer interferometry (BLI)

Binding of LL-37 and its functional analogue CRAMP to DNA was analyzed using an Octet N1 bio-layer interferometry (BLI) system (Sartorius). Biotinylated DNA was immobilized on high-precision streptavidin (SAX) biosensors (Octet® High Precision Streptavidin Biosensors, Sartorius) by incubation in a 50 µg/mL DNA solution for 3 min. Following immobilization, biosensors were washed with assay buffer to remove unbound ligand. Kinetic measurements were performed at room temperature under continuous agitation (1000 rpm) in 10 mM HEPES (pH 7.4), 150 mM NaCl, and 0.05% surfactant P20. DNA-loaded biosensors were immersed in LL-37 or CRAMP solutions for a 120 s association phase, followed by a 120 s dissociation phase in assay buffer. Biosensors were regenerated using 2 M NaCl for 30 s prior to reuse. To assess the effect of pH on peptide-DNA interactions, LL-37 binding experiments were additionally performed in 10 mM sodium acetate buffer (pH 6.0) or 10 mM Tris-HCl buffer (pH 8.0), each supplemented with 150 mM NaCl and 0.05% surfactant P20. Scrambled LL-37 (LL-37 scr) and biotin-coated SAX biosensors lacking immobilized DNA were used as controls for non-specific binding. Binding kinetics were analyzed using a 1:1 Langmuir binding model implemented in Octet Analysis Studio software (Sartorius). For competition experiments, LL-37 or CRAMP was pre-incubated with ApoA-I for 20 min at room temperature before exposure to DNA-coated biosensors. ApoA-I was used at molar ratios ranging from 0.5 to 4 relative to LL-37 or CRAMP. ApoE was included as an additional apolipoprotein control to assess the specificity of the inhibitory effect.

Gel retardation assay

Gel retardation assay
Purified genomic DNA (3 µg/mL) was incubated with LL-37 (45 µg/mL) for 10 min at room temperature to allow complex formation[13]. ApoA-I was subsequently added to preformed LL-37-DNA complexes at LL-37:ApoA-I molar ratios of 1:1, 1:2, and 1:4, followed by incubation for 20 min at room temperature. Complex formation was assessed by electrophoretic mobility shift assay using 1% agarose gels. To evaluate the effect of ApoA-I on the susceptibility of LL-37-DNA complexes to nuclease degradation, complexes were incubated with DNase I (19.22 µg/mL; A&A Biotechnology) for 60 min at 37°C. DNase I was subsequently inactivated at 75°C for 10 min. The integrity of DNA and the protective capacity of peptide-DNA complexes were evaluated by agarose gel electrophoresis.

PicoGreen Fluorescence Assay

Purified genomic DNA (3 µg/mL) was incubated with LL-37 (45 µg/mL) for 10 min at room temperature to allow complex formation[13]. ApoA-I was subsequently added at LL-37:ApoA-I molar ratios ranging from 1:1 to 1:60 and incubated for an additional 20 min. Free DNA was quantified using Quant-iT™ PicoGreen™

dsDNA reagent (Invitrogen) according to the manufacturer's instructions. Fluorescence emission spectra (500–600 nm) were recorded following excitation at 485 nm.

Cell culture

pDCs were isolated from PBMCs with BD IMAG Cell Separation System (BD Biosciences). PBMCs were first separated from human peripheral blood by using density gradient centrifugation, and pDCs were obtained following a manufacturer's protocol. pDCs were then seeded at 8×10^5/well in 200 µl of complete medium (RPMI 1640 medium supplemented with 10% FBS and 50 µg/mL gentamicin). During experiments we used CpG oligonucleotides, which are short single-stranded DNA molecules that mimic bacterial DNA. Oligonucleotides CpG ODN 2216, which are a class A of CpG were chosen for our research while it is known that they elicit higher and longer production of IFN-α in pDCs compared to CpG class B. The cells were stimulated with DNA alone, LL-37, and ApoA-I, as well as with LL-37:DNA complexes and these complexes treated with ApoA-I. Before cell stimulation, LL-37 and DNA were mixed in PBS for 10 min at the indicated concentrations: DNA (final concentration, 3 µM) and LL-37 (final concentration, 28.8 µg/mL) at a 1:1 molar ratio. Subsequently, ApoA-I was added to the complexes at a LL-37:ApoA-I molar ratio of 1:2, followed by incubation for 20 min prior to cell stimulation. Subsequently, cells were incubated with all factors for 15 min, washed with PBS three times, and incubated in fresh complete medium overnight at 37˚C in a humidified 5% CO_2 atmosphere. Cell morphology was visualized by bright-field microscopy, and images were taken before culture supernatants were collected for cytokine measurement by ELISA, and cells were collected for RNA isolation and qPCR analysis.

Primary Normal Human Epidermal Keratinocytes, neonatal (HEKn) were seeded at 1.25×10^5/well into rat type I collagen coated wells in 500 µl of EpiLife medium without EpiLife Defined Growth Supplement and incubated overnight at 37˚C in a humidified 5% CO_2. To stimulate HEKn cells, we used polyinosinic-polycytidylic acid (poly(I:C)), a synthetic analog of dsRNA and a TLR3 agonist, which is commonly employed to model the effects of extracellular dsRNA. The cells were stimulated with RNA alone, LL-37 ApoA-I, LL-37:RNA complexes, or ApoA-I treated LL-37:RNA complexes. Prior to cell stimulation, LL-37 and RNA were mixed in PBS for 10 min at the indicated concentrations: RNA (final concentration, 4 µg/mL) and LL-37 (final concentration, 9 µg/mL), corresponding to a 0.01:1 molar ratio. ApoA-1 (270 µg/mL) was subsequently added to the complexes, followed by an additional 20 min incubation before cell stimulation. Cells were incubated for 4 h under standard culture conditions. Total RNA was then isolated from the cells and subjected to qPCR analysis.

Human neutrophils were isolated from peripheral blood as previously described[47]. Purified cells were resuspended in phenol red-free DMEM, seeded onto poly-L-lysine-coated plates at a density of 2×10^6 cells per well, and maintained at 37°C in a humidified atmosphere containing 5% CO_2 until stimulation.

Flow cytometry

pDCs (0.8×10^5 cells/mL) were incubated with a mixture of FITC-CpG (1.3 µg/mL) and LL-37 (6 µg/mL) for 15 min, or with LL-37:DNA complexes containing ApoA-I at a 1:2 molar ratio of LL-37 to ApoA-I. Cells were washed three times with PBS, and uptake of the complexes was determined by measuring the fluorescence intensity with flow cytometry (BD Biosciences). The mean fluorescence intensity of cells labeled with FITC-conjugated CpG was measured in each group.

IMQ-induced psoriasisform skin inflammation model in mice

Mice were housed in individually ventilated cages under specific pathogen-free conditions and provided with standard laboratory chow and water ad libitum. Animals were maintained under controlled environmental conditions (12 h light/12 h dark cycle, 22°C, and 60% relative humidity) at the animal facility of the Faculty of Biochemistry, Biophysics and Biotechnology, Jagiellonian University (Krakow, Poland). All animal procedures were conducted in accordance with Directive 2010/63/EU of the European Parliament on the protection of animals used for scientific purposes and were approved by the 2nd Local Institutional Animal Care and Use Committee in Krakow (permit no. 856A/2024).

Psoriasisform skin inflammation was induced as previously described[48]. Briefly, 6-8-week-old C57BL/6 mice received a daily topical application of 62.5 mg of commercially available 5% imiquimod cream (Aldara®, 3M Pharmaceuticals) to the shaved dorsal skin for five consecutive days. Control animals received vehicle treatment (Vaseline). Beginning on day 1 of the experiment, ApoA-I (800 µg/mL; 50 µL per dose) was administered daily by either intradermal (i.d.) or intraperitoneal (i.p.) injection, according to the experimental design shown in Fig. 4C. The severity of skin inflammation was evaluated using a modified Psoriasis Area and Severity Index (PASI) scoring system, assessing erythema, scaling, and skin thickening on a scale from 0 to 4 (none, slight, moderate, marked, and very marked). Dorsal skin thickness was additionally measured daily using a digital micrometer. At the end of the treatment period, mice were euthanized by anesthetic overdose, and skin samples were collected for further analyses.

Transepidermal Water Loss (TEWL) Measurement

Epidermal barrier integrity was assessed by measuring transepidermal water loss (TEWL) using a Tewameter® TM 300 (Courage + Khazaka Electronic GmbH). Measurements were performed under controlled environmental conditions of temperature and relative humidity. The probe was placed directly above the tissue surface, and measurements were recorded for at least 60 s until stable and reproducible values were obtained. Each sample was measured in triplicate, and the final TEWL value was calculated as the mean of the three measurements and expressed in g/ m^2/h.

Three-Dimensional Human Psoriatic Skin Model

A three-dimensional human psoriatic skin model (Psoriasis Tissue Model, SOR-300-FT; MatTek Corporation) was used to examine the effects of ApoA-I on skin tissue responses. Tissue inserts were maintained according to the manufacturer's instructions. Unstimulated tissues cultured under identical

conditions served as the control (Model) group. Following a 48 h equilibration period, tissues were stimulated either apically or basolaterally with ApoA-I (270 µg/mL), ApoE (270 µg/mL), or calcipotriol (60 ng/mL). After 48 h, stimulation was repeated under identical conditions. Following an additional 48 h incubation period, culture media and tissue samples were collected for downstream analyses. Tissue specimens were processed for histological evaluation, whereas culture supernatants were used for the quantification of cytokine and chemokine production.

Cytokine and chemokine measurement

Cytokine production by pDCs was quantified using enzyme-linked immunosorbent assays (ELISAs). Cell culture supernatants were collected and concentrations of human IFN-α (PBL Assay Science) and IL-6 (BD OptEIA, BD Biosciences) were determined according to the manufacturers' instructions. Cytokine and chemokine production by the 3D human skin model was assessed using the Human Inflammatory Cytokine Cytometric Bead Array (CBA) Kit (BD Biosciences). Concentrations of CXCL8, CXCL10 and CCL2 in culture supernatants were determined according to the manufacturer's instructions and analyzed on a BD LSRFortessa™ flow cytometer (BD Biosciences). Levels of IL-6 and IL-36γ (R&D Systems) were measured separately using ELISA kits according to the manufacturers' instructions.

Quantitative Real-Time PCR Analysis

Total RNA from pDCs and HEKn was isolated using TRI Reagent (Sigma-Aldrich). Total RNA from murine skin samples was isolated using the mirVana™ RNA Isolation Kit (Thermo Fisher Scientific) according to the manufacturer's instructions. RNA was reverse-transcribed using a High-Capacity cDNA Reverse Transcription Kit (Applied Biosystems). For human samples, cDNA was synthesized from 800 ng of total RNA in a final volume of 20 µL. Quantitative PCR reactions were performed in a final volume of 15 µL containing 5 µL of cDNA, 10 µM forward and reverse primers, and 1× GoTaq qPCR Master Mix (Promega). The amplification protocol consisted of an initial denaturation step at 95°C for 5 min, followed by 40 cycles of 95°C for 30 s, 60°C for 30 s, and 72°C for 45 s, with a final extension at 72°C for 10 min. For murine samples, 1,000 ng of total RNA was reverse-transcribed, and five-fold diluted cDNA (3 µL per reaction) was used for qPCR analysis under conditions specified for individual targets (Table 2). Human and mouse primer sequences are listed in Tables 1 and 2, respectively. Relative gene expression was calculated using the $\Delta\Delta C_T$ method[49]. Elongation factor 2 (EF-2) was used as the reference gene for normalization. The specificity of amplification products was confirmed by melt curve analysis.

Table 1
Primer sequences used for RT-qPCR analysis of human genes.

Gene	GenBank Accession	Sequence (5'→3')	Product lenght
EF-2 F	NM_001961.4	GACATCACCAAGGGTGTGCAG	215 bp
EF-2 R		TTCAGCACACTGGCATAGAGGC	
MxA F	NM_001438334.1	ACTCTGTCCAGCCCCGTAGAC	149 bp
MxA R		TCACAGCTTCCTGCTAAATCACC	
IFN-β1 F	NM_002176.4	CTTGGATTCCTACAAAGAAGCAGC	146 bp
IFN-β1 R		TCCTCCTTCTGGAACTGCTGCA	

Table 2
Primer sequences used for RT-qPCR analysis of murine genes.

Gene	GenBank Accession	Sequence (5'→3')	Product lenght	Annealing temp. (°C)
EF-2 F	NM_007907.3	GACATCACCAAGGGTGTGCAG	214 bp	58
EF-2 R		TCAGCACACTGGCATAGAGGC		
S100a8 F	NM_013650.2	CAAGGAAATCACCATGCCCTC	176 bp	62
S100a8 R		GCCACACCCACTTTTATCACCA		
Ly6G F	NM_001374230.1	GACTTCCTGCAACACAACTACC	162 bp	60
Ly6G R		ACAGCATTACCAGTGATCTCAGT		
Lcn2 F	NM_008491.2	GAACTTGATCCCTGCCCCAT	236 bp	62
Lcn2 R		TTCTGATCCAGTAGCGACAGC		
Il17a F	NM_010552.3	CAGGGAGAGCTTCATCTGTGT	94 bp	60
Il17a R		GCTGAGCTTTGAGGGATGAT		
Il1β F	NM_008361.4	TGCCACCTTTTGACAGTGATG	138 bp	60
Il1β R		TGATGTGCTGCTGCGAGATT		
Il6 F	NM_001314054.1	AAGAAATGATGGATGCTACCAAACTG	79 bp	60
Il6 R		GTACTCCAGAAGACCAGAGGAAATT		

Histology and Hematoxylin and Eosin Staining

Skin tissue samples were rinsed in phosphate-buffered saline (PBS) and maintained in PBS for 20 h at 4°C prior to processing. Samples were subsequently dehydrated through a graded ethanol series, cleared

in xylene, embedded in paraffin, and sectioned at a thickness of 6 µm using a rotary microtome. Sections were mounted on poly-L-lysine-coated glass slides and dried at 37°C. Prior to staining, paraffin was removed by xylene treatment and sections were rehydrated through a descending ethanol series. Histological evaluation was performed using hematoxylin and eosin (H&E; Sigma-Aldrich) staining according to standard protocols. After staining, sections were dehydrated, cleared in xylene, and coverslipped using a xylene-based mounting medium. Histological images were acquired using an Axio Observer microscope (Zeiss) equipped with a 20× objective.

Immunofluorescence Staining

Paraffin-embedded tissue sections (5 µm) were deparaffinized in xylene, rehydrated through a graded ethanol series, and subjected to heat-induced antigen retrieval in citrate buffer (10 mM sodium citrate, 0.05% Tween-20, pH 6.0) for 15 min at 95°C. Sections were washed with PBS, permeabilized with 0.1% Triton X-100 in PBS for 15 min, and blocked with 5% goat serum in PBS for 2 h at room temperature. For the IMQ-induced psoriasisform skin inflammation in mice, tissue sections were incubated with rat anti-mouse Ly6G (1:200, Cell Signaling Technology) and rabbit anti-mouse PCNA (1:100, Cell Signaling Technology) primary antibodies for 1 h at room temperature. Following washing, sections were incubated with Alexa Fluor 568-conjugated goat anti-rat IgG (Abcam) and Alexa Fluor 488-conjugated goat anti-rabbit IgG (1:500, Cell Signaling Technology) secondary antibodies for 1 h at room temperature. For the 3D human psoriatic skin model, tissue sections were incubated for 2 h at room temperature with rabbit anti-human cytokeratin 13 (1:100, Abcam), rabbit anti-human vimentin (1:100, Abcam), rabbit anti-human β-defensin 2 (1:100, Invitrogen), or rabbit anti-human psoriasin (1:50, Proteintech) primary antibodies. Following washing, sections were incubated with Alexa Fluor 488-conjugated goat anti-rabbit IgG secondary antibody (1:1000, Cell Signaling Technology) for 1 h at room temperature. Nuclei were counterstained with DAPI using ProLong™ Gold Antifade Mountant (Thermo Fisher Scientific). Fluorescence images were acquired using an Axio Observer fluorescence microscope (Zeiss) equipped with a 20× objective. Fluorescence intensity was quantified using ImageJ software.

SYTOX Green Staining

Paraffin-embedded murine skin sections were deparaffinized, rehydrated, and permeabilized as described above. Sections were subsequently washed with Hank's Balanced Salt Solution (HBSS) supplemented with Ca^{2+} and Mg^{2+} and incubated with SYTOX™ Green nucleic acid stain (167 nM; Invitrogen) for 15 min at room temperature. Following staining, sections were mounted using Dako Fluorescence Mounting Medium (Dako). Images were acquired using a Stellaris confocal microscope (Leica Microsystems).

Mass spectrometry

Protein samples (20 µg) were prepared for LC-MS/MS analysis using SP3 sample preparation protocol[50]. Resulting peptides were suspended in 0.1% formic acid (FA) and 250 ng of peptide mixture was analysed with Astral Orbitrap mass spectrometer coupled to Vanquish Neo UHPLC (both Thermo Fisher Scientific). UHPLC was operated in a direct injection mode. Peptides were separated using Aurora

Ultimate XT 25 cm × 75 µm C18 column (IonOpticks) in 60 min gradient of acetonitrile (ACN) at a flow rate of 0.5 µl/min at 55°C. The gradient consisted of 3 major steps: 2%-10% B 10 min, 10%-25% B 32 min, 25%-45% B 18 min (buffer B: 80% ACN, 0.1% FA; buffer A: 0.1% FA). The eluting peptides were analysed with Orbitrap Astral mass spectrometer using DIA method. Data were collected within 200 windows of 3-Th for the precursors from the mass range of 380–980 m/z. The maximum injection time (IT) was set to 5 ms and normalized AGC target to 500%. The isolated ions were fragmented with the normalized collision energy set to 25%. Astral scan range was 150–2000 m/z. Additionally, full-MS spectra were acquired every 0.6 s with the resolution of 240000, scan range of 380–980 m/z, maximum IT of 3 ms and normalized AGC target of 500%.

Raw files were analysed in DIA-NN 2.1.0[51] using in silico DIA-NN predicted spectral library generated from mouse reference proteome (UniProtKB, 21 756 sequences, downloaded in June 2025). The DIA-NN spectral library building as well as search were performed using the following settings: protease – Trypsin/P, missed cleavages – up to 1, maximum number of variable modifications – 2, modifications – C carbamidomethylation, N-term M excision, M oxidation, protein N-terminal acetylation, peptide length range – 7–30, precursor charge range – 2–4, precursor m/z range 380–980, fragment ion m/z range – 150–2000, mass accuracy – 10 ppm, MS1 accuracy – 4 ppm, scan window – 7, scoring – peptidoforms, proteotypicity – genes, machine learning – NNs (cross-validated), quantification strategy – QuantUMS (high precision), cross-run normalisation – RT-dependent, library generation – IDs, RT & IM profiling, speed and RAM usage – optimal results. MBR and protein inference were enabled. The resulting pg_matrix was filtered for protein groups that satisfy Global.PG.Q.Value threshold of 0.01. The list of protein groups that meet this criterion was obtained by filtering the main output file in Rstudio (v2024.12.1 + 563). Then, non-mouse cRAP proteins were excluded. Data matrix was further processed in Perseus (v2.1.4.0)[52]. Protein intensity values were log2 transformed and matrix was filtered for proteins that had a minimum 70% of valid values in at least one group. Then, remaining missing values were imputed by constant low value. In order to reveal changes between the groups, Student’s t-test with Benjamini-Hochberg FDR set to 0.05 was used. Proteins that satisfied threshold of q-value < 0.05 and the abundance change of at least 20% were considered differential.

Cytotoxicity assay

Cytotoxicity was assessed using the CytoTox 96 Non-Radioactive Cytotoxicity Assay (Promega), which quantifies the release of lactate dehydrogenase (LDH) from cells with compromised membrane integrity. Plasmacytoid DCs and HEKn were incubated with ApoA-I under the indicated experimental conditions. Following stimulation, cell-free supernatants were collected and analyzed according to the manufacturer's instructions. Absorbance was measured at 490 nm using a microplate reader. Maximum LDH release from completely lysed cells and spontaneous LDH release from untreated cells were used as positive and negative controls, respectively. Cytotoxicity was expressed as the percentage of LDH release relative to the maximum lysis control.

Cytospin preparation and trypan blue staining

Freshly isolated or ApoA-I-stimulated pDCs were collected by centrifugation (300 × g, 10 min, 4°C) and resuspended in Ca^{2+}- and Mg^{2+}-free PBS. Cell suspensions were gently mixed immediately before cytospin preparation to ensure homogeneous cell distribution. Cytospin slides were prepared using 2 × 10^5 cells per sample and centrifuged onto glass slides using a Shandon™ Cytospin™ 3 cytocentrifuge (Thermo Fisher Scientific) at 400 rpm for 10 min at room temperature. The resulting preparations were stained with trypan blue and examined by light microscopy.

Quantification and visualization of neutrophil extracellular traps (NETs)

Neutrophils (2 × 10^6 cells) were stimulated for 3 h with LL-37 (1 µg/mL), ApoA-I (30 µg/mL), or LL-37:ApoA-I complexes. To release cell-associated NETs, samples were treated with micrococcal nuclease (1 U/mL, 15 min, Thermo Fisher Scientific) and centrifuged (1,800 × g, 10 min, room temperature). NET-derived extracellular DNA in the supernatants was quantified using SYTOX Green (Thermo Fisher Scientific) and measured fluorometrically (Ex 485 nm, Em 535 nm), with results expressed as relative fluorescence units (RFU). For NET visualization, neutrophils (1 × 10^5 cells) were seeded onto poly-L-lysine-coated coverslips, allowed to adhere for 30 min, and stimulated for 3 h with LL-37 (1 µg/mL), ApoA-I (30 µg/mL), or LL-37:ApoA-I complexes. Cells were fixed with 3.7% formaldehyde, blocked, permeabilized with 0.1% saponin, and stained with anti-human neutrophil elastase primary antibodies (Athens Research & Technology) followed by APC-conjugated secondary antibodies (Jackson ImmunoResearch Laboratories). DNA was counterstained with DAPI-containing mounting medium (Thermo Fisher Scientific), and NET structures were imaged using an Axio Observer fluorescence microscope (Zeiss) equipped with a 40× objective.

Statistical Analysis

Statistical analyses were performed using GraphPad Prism 11 software (GraphPad Software). Comparisons between two groups were performed using an unpaired two-tailed Student's t-test. Comparisons among multiple groups were performed using one-way or two-way analysis of variance (ANOVA), followed by Šídák's or Bonferroni's multiple-comparisons post hoc test, as indicated in the corresponding figure legends. Data are presented as mean ± SD or mean ± SEM, as specified in the figure legends. Relative differences were considered statistically significant at $p < 0.05$. Statistical significance is indicated as follows: $p < 0.05$ (*), $p < 0.01$ (**), $p < 0.001$ (***), and $p < 0.0001$ (****).

Results

LL-37 complexed with ApoA-I does not interact with nucleic acids

To delineate the molecular basis of the ApoA-I:LL-37 interaction, we performed protein-peptide docking and atomistic molecular dynamics (MD) simulations. Unbiased docking was conducted using a

truncated monomeric human ApoA-I crystal structure (PDB: 1AV1) and an AlphaFold-generated LL-37 model, followed by MD simulations and mapping of LL-37 contact sites on ApoA-I (Fig. 1A). Each docking configuration was subjected to 200 ns of simulations to evaluate binding stability. No single consensus binding site was identified; instead, LL-37 exhibited distributed binding along the ApoA-I backbone, with a pronounced enrichment of interaction sites within the N-terminal half of the protein. Nine of the ten generated ApoA-I:LL-37 complexes involved interactions within the N-terminal half of ApoA-I. RMSD progression (Fig. 1B) and MM/PBSA binding free-energy calculations (Fig. 1C) revealed substantial variability in complex stability across models. Notably, model 9 displayed the lowest RMSD fluctuations and the most favourable MM/PBSA binding free energy, consistent with stabilization through adoption of a compact complex architecture. Collectively, these findings support the notion of ApoA-I as a versatile biological scaffold capable of efficiently accommodating LL-37 along multiple binding modes, consistent with its role as a physiologically relevant scavenger of this antimicrobial peptide.

Considering the previously documented phenomenon of ApoA-I binding to human cathelicidin LL-37 with the dissociation constant (*KD*) in the low-micromolar range[34], we hypothesized that such interaction can prevent its binding to nucleic acids. To test this assumption, we applied the bio-layer interferometry (BLI) method to measure the kinetics and determine the binding parameters of LL-37 alone and complexed with ApoA-I to DNA. Initially, using nucleic acid immobilized on a SAX biosensor we estimated the *KD* values for LL-37 showing that *KD* remained in the low micromolar range and did not differ significantly under the tested pH conditions (6.0, 7.4 and 8.0) [Table 3, Fig. 2A]. This observation clearly indicates that the peptide's overall affinity for DNA remains broadly stable across the examined pH range. To assess non-specific interactions, scrambled LL-37 (LL-37 scr), which has the same amino acid composition as LL-37 but a randomized sequence, was used as a control [Fig. 2B]. Then, using an optimized model we tested the efficiency of DNA binding by LL-37 complexed with ApoA-I. For that purpose, we preincubated LL-37 with ApoA-I before contacting the complex with the immobilized DNA [Fig. 2C]. ApoA-I was applied at molar ratio ranging from 0.5 to 4 relative to LL-37, under three distinct pH conditions (6.0, 7.4 and 8.0) [Fig. 2C]. The binding analysis revealed that the molar ratio of LL-37 to ApoA-I at which LL-37 binding is reduced by half is 1.120 at pH 7.4, 1.058 at pH 8.0, and 1.121 at pH 6.0 [Fig. 2E]. Application of 2:1 molar excess of ApoA-I over LL-37 resulted in a 64.5% reduction in LL-37 binding to DNA. In comparison, ApoE, which was used to determine specificity of the interaction [Fig. 2D] at the same excess to LL-37 (2:1) inhibited the LL-37:DNA interaction by only 12.8% [Fig. 2F]. In summary, we demonstrated that the presence of ApoA-I specifically and efficiently inhibits the interaction between LL-37 and DNA. ApoA-I acted as a strong competitor, reducing DNA binding by 50% at a 1:1 molar ratio of LL-37 to ApoA-I, across all tested pH conditions.

Table 3
Kinetic and binding parameters for the interactions of LL-37 with immobilized DNA, determined by BLI measurements. All parameters are presented with the standard error.

LL-37, pH 6.0	***KD* (M)**	***ka* (1/Ms)**	***kd* (1/s)**
	$4.40 \times 10^{-6} \pm 7.10 \times 10^{-7}$	**$3.66 \times 10^{3} \pm 2.71 \times 10^{2}$**	**$1.61 \times 10^{-2} \pm 2.31 \times 10^{-3}$**
LL-37, pH 7.4	$2.98 \times 10^{-6} \pm 9.01 \times 10^{-8}$	$5.04 \times 10^{3} \pm 1.48 \times 10^{2}$	$1.50 \times 10^{-2} \pm 1.09 \times 10^{-4}$
LL-37, pH 8.0	$5.65 \times 10^{-6} \pm 3.03 \times 10^{-7}$	$1.03 \times 10^{3} \pm 5.98 \times 10^{2}$	$5.82 \times 10^{-3} \pm 3.71 \times 10^{-4}$

ApoA-I promotes dissociation of LL-37:nucleic acid complexes

Subsequently, we investigated whether ApoA-I can dissociate pre-formed LL-37:nucleic acid complexes. Using a classical electrophoretic mobility shift assay (EMSA), we showed that the addition of ApoA-I at LL-37:ApoA-I ratios of 1:1 or 1:2 did not alter the migration of the LL-37:DNA complex. A mobility shift was observed only at a four-fold excess of ApoA-I relative to LL-37 [Fig. 2G]. Under these conditions, DNA released from the complex migrated similarly to free DNA, indicating dissociation of nucleic acids previously complexed with LL-37. These results demonstrate that ApoA-I efficiently competes with nucleic acids for binding to LL-37, preferentially forming LL-37:ApoA-I complexes. Dissociation of DNA and RNA from LL-37:nucleic acid complexes in the presence of ApoA-I was further confirmed by spectral analysis [Fig. 2H, I]. Fluorescence emitted by unbound DNA was significantly higher compared to samples in which nucleic acids were complexed with LL-37. Notably, addition of ApoA-I reversed the inhibition of fluorescence emission, restoring levels comparable to those of free DNA at 30- and 60-fold molar excesses of ApoA-I over LL-37 [Fig. 2I]. Given the ability of ApoA-I to dissociate LL-37:nucleic acid complexes, we next demonstrated that the released nucleic acids could subsequently be degraded by nucleases [Fig. 2J]. Taken together, these data show that ApoA-I efficiently promotes dissociation of LL-37:nucleic acid complexes. Moreover, nucleic acids released from LL-37 complexes may subsequently undergo nuclease-mediated degradation, thereby limiting their accumulation.

ApoA-I efficiently prevents inflammation induced by LL-37:nucleic acid complexes

LL-37 binds self-DNA fragments released from dying cells and promotes their translocation into the endocytic pathway of plasmacytoid dendritic cells (pDCs), thereby bypassing a safety mechanism that normally discriminates between pathogenic and self-nucleic acids. This mechanism relies on the intracellular localization of TLR9. Consequently, self-DNA complexes are efficiently deposited in early endosomes (EEs), triggering TLR9 signaling and leading to sustained type I IFN production. As pDC-derived IFN-α has been shown to be essential for the development of psoriasis in vivo, we applied this model to investigate whether ApoA-I could abrogate the immunogenicity of LL-37:nucleic acid complexes [Fig. 3A]. As shown in Fig. 4B, stimulation of pDCs with DNA resulted in the formation of

pronounced cell clusters, indicating cellular activation. This effect was further intensified upon exposure to LL-37:DNA complexes, whereas the addition of ApoA-I significantly reduced the number of cell aggregates. To elucidate the mechanisms underlying these morphological changes, we performed a comprehensive analysis of inflammatory mediator expression, focusing on IFN-α and IL-6 [Fig. 3C, D]. We confirmed that LL-37:DNA complexes induce robust IFN-α production by pDCs without concurrent IL-6 secretion, consistent with selective activation of TLR9 in early endosomes. Notably, the presence of ApoA-I markedly suppressed IFN-α production while promoting IL-6 secretion. To further confirm differential regulation of the type I IFN pathway, we examined the expression of MxA, a key effector protein of the type I IFN response. Analysis of MxA mRNA expression corroborated the IFN-α protein data [Fig. 3E]. Collectively, these findings demonstrate that ApoA-I disrupts the aggregated structure of LL-37:DNA complexes, suppressing IFN-α production and downstream type I IFN signaling while promoting IL-6 secretion. Although pDC responses to LL-37:DNA complexes were strongly donor-dependent, ApoA-I alone did not elicit a pro-inflammatory response in any donor examined nor was it cytotoxic [**Supplementary Fig. 1]**. Furthermore, flow cytometric analysis demonstrated that ApoA-I markedly inhibited the intracellular uptake of LL-37:DNA complexes by pDCs, resulting in attenuation of the inflammatory response [Fig. 3F, G]. While type I IFN production in the skin was initially attributed to classical immunocytes such as dendritic cells, it is now recognized that epidermal keratinocytes also contribute to this process and play a critical role in initiating cutaneous inflammation. In particular, IFN-β is abundantly produced by epidermal keratinocytes during psoriasis and wound healing, where it enhances DC function and promotes T-cell activation[22]. Based on these observations and our results in pDCs [Fig. 3A-G], we next employed a culture model of primary neonatal human epidermal keratinocytes (HEKn cells) to assess whether ApoA-I could similarly abrogate type I IFN production in response to LL-37:RNA complexes [Fig. 3H]. Consistent with our findings in pDCs, ApoA-I significantly inhibited LL-37:RNA-induced IFN-β production in HEKn cells [Fig. 3I]. This effect was associated with reduced nucleic acid translocation into endosomal compartments and diminished TLR activation. Together, these results demonstrate that ApoA-I exerts broad immunomodulatory activity that is independent of nucleic acid type and is conserved across multiple skin-relevant cell types.

ApoA-I treatment alleviates psoriasiform inflammation in IMQ-treated mice

Given that the pro-inflammatory effects of LL-37 have been documented in psoriatic skin[6], we sought to investigate the *in vivo* therapeutic effect of ApoA-I using an imiquimod (IMQ)-induced mouse model of psoriasis. As the murine homolog of human LL-37 is CRAMP, a peptide with similar activity but a distinct amino acid sequence (sharing 47% sequence identity and 67% sequence similarity[7]), we first examined the ability of ApoA-I to dissociate CRAMP:DNA complexes using the BLI method. We performed an analysis analogous to that conducted for LL-37 **[**Fig. 2C**]**, this time using CRAMP **[**Fig. 4A**]**. The analysis revealed that the molar ratio of CRAMP to ApoA-I required to achieve a 50% reduction in binding to DNA is 0.2278, confirming the markedly higher efficiency of ApoA-I in inhibiting CRAMP:DNA interactions relative to LL-37 [Fig. 4B]. To induce psoriasis-like skin inflammation IMQ was applied topically to the

shaved backs of mice for five consecutive days (d0 – d4) [Fig. 4C]. The application of IMQ rapidly induces a dermatitis closely resembling human psoriasis[48]. IMQ-treated mice displayed significantly scaly, erythematous and thickened skin lesions compared to control mice [Fig. 4D, E, F]. Those changes resulted in higher Psoriasis Area and Severity Index (PASI) scores in IMQ-treated mice [Fig. 4E]. Starting from day 1 of the experiment (d1) ApoA-I was applied daily (i.d. or i.p.) in the control and psoriatic skin of IMQ mice [Fig. 4C]. Administration of ApoA-I at doses up to 800 µg/mL did not alter skin physiology [Fig. 4D] and showed no signs of hepatotoxicity in mice. In addition, no splenomegaly was observed [**Supplementary Fig. 2**] and body weight was not affected [Fig. 4G]. During the treatment period (d1 – d4) ApoA-I application (i.d. or i.p.) displayed therapeutic efficacy on mouse psoriatic skin as showed by the reduction of scales, erythema and skin thickness as well as significantly lower cumulative PASI score [Fig. 4D, E, F]. To further confirm the effect of ApoA-I, we performed a histochemical analysis of the skin collected from the backs of mice on day 4 of the experiment. In psoriatic skin lesions from IMQ-treated mice, we observed characteristic psoriasiform histopathological changes, including epidermal acanthosis and hyperkeratosis [Fig. 4H]. Furthermore, the epidermal rete ridges, marked with asterisks in the dermis layer, [Fig. 4H] were significantly elongated, club-shaped, extending into the dermis layer. In contrast, both intradermal (i.d.) and intraperitoneal (i.p.) administration of ApoA-I ameliorated the dermatitis, as evidenced by reduced skin and epidermal thickness and less pronounced elongation of the rete ridges, Transepidermal water loss (TEWL), an indicator of epidermal barrier function, was measured on the dorsal skin on days 3 and 4. Both routes of ApoA-I administration significantly attenuated the IMQ-induced increase in TEWL [Fig. 4J]. Furthermore, immunohistochemical staining was performed to study the expression of the proliferation marker, PCNA (Proliferating Cell Nuclear Antigen). As expected, IMQ treatment markedly increased the number of PCNA-positive cells in the basal and superbasal layer of the epidermidis. In contrast, ApoA-I treatment significantly reduced PCNA expression to levels comparable to those observed in control mice [Fig. 4K]. This reduction is comparable to the control group of mice. Collectively, the morphological and histological findings demonstrate that ApoA-I treatment alleviates IMQ-induced psoriasiform skin inflammation in mice.

ApoA-I attenuates inflammation and restore homeostasis in imiquimod-induced psoriasis model

Psoriasis is characterized by increased neutrophil infiltration into both the epidermis and dermis, which contributes to the development of inflammatory lesions[27, 53]. Immunohistochemical staining for neutrophils ($Ly6G^+$) revealed massive infiltration of these cells into the upper dermal layer within lesional areas following IMQ treatment [Fig. 5A,B]. Notably, neutrophil accumulation was significantly reduced upon administration of ApoA-I, both intradermally (i.d.) and intraperitoneally (i.p.). This observation was further confirmed by the downregulation of transcripts considered neutrophil markers, including *S100a8*, *Ly6G*, and *Lcn2* [Fig. 5C-E]. In parallel with leukocyte infiltration in psoriatic tissue, increased accumulation of proinflammatory cytokines is observed, particularly those belonging to the IL-1 family and the IL-23/Th17 pathway[53, 54]. Real-time PCR analysis demonstrated that ApoA-I administration (i.d. and i.p.) in psoriatic mice significantly reduced the expression of cytokine transcripts *Il17A*, *Il1β*, and *Il6*

[Fig. 5F–H]. These effects correlated with a reduction in cell-free DNA (cfDNA) in psoriatic skin upon ApoA-I treatment (i.d. and i.p.) [Fig. 5I, J], as evidenced by a decreased presence of diffuse, scattered, or point-like cfDNA structures (indicated by arrows in Fig. 5I). To further characterize the molecular changes induced by ApoA-I, a comprehensive proteomic profiling using mass spectrometry was performed. Principal component analysis (PCA) revealed clear clustering of samples according to experimental groups [Fig. 5K]. Notably, 365 proteins upregulated during IMQ-induced inflammation were restored toward baseline levels following ApoA-I treatment [Fig. 5L]. Moreover, ApoA-I administration led to the upregulation of several proteins critical for skin architecture and tissue repair, including Panx3, Srcin1, Elovl3, and Krt79 [Fig. 5M]. In conclusion, these data demonstrate that ApoA-I restores molecular homeostasis in the skin, thereby effectively alleviating the pathological features of psoriasis.

ApoA-I meliorates psoriasiform features in a 3D human skin model

The above experiments in the IMQ-induced murine model of psoriasis demonstrated that ApoA-I efficiently alleviates psoriasiform inflammation. To further assess its translational potential, we employed a 3D human psoriasis model comprising keratinocytes and fibroblasts isolated from psoriatic lesions [Fig. 6A]. Together, these cells form a multilayered, highly differentiated tissue containing a desquamating surface layer. In this model, ApoA-I was applied either apically or basolaterally [Fig. 6A] twice at 48-hour intervals. Analysis of the thickness of individual skin layers revealed that ApoA-I reduced the thickness of the cornified layer without detectably affecting epidermal thickness [Fig. 6B]. Moreover, ApoA-I exerted anti-inflammatory effects by inhibiting the production of the chemokines CXCL8/IL-8 and CCL2/MCP-1 following both apical and basolateral application [Fig. 6C]. This effect was specific to ApoA-I, as ApoE did not influence the expression of these chemokines [**Supplementary Fig. 3**]. Using immunohistochemical staining, we next assessed whether ApoA-I modulates the expression of established psoriasis biomarkers, including human β-defensin-2 (HBD-2) and psoriasin/S100A7. Both apical and basolateral administration of ApoA-I efficiently suppressed the expression of HBD-2 and psoriasin/S100A7 [Fig. 6D]. Next, the therapeutic effects of ApoA-I were compared with those of calcipotriol, a synthetic derivative of calcitriol (vitamin D) that is widely used in the treatment of psoriasis [**Supplementary Fig. 4**]. Apical application of calcipotriol, administered twice at 48-hour intervals, inhibited the production of a broad range of chemokines and cytokines but did not exhibit the selective effects observed for ApoA-I. Similar to ApoA-I, calcipotriol treatment resulted in reduced immunoreactivity for HBD-2 and psoriasin/S100A7 [**Supplementary Fig. 4**]. Notably, ApoA-I suppressed HBD-2 expression in psoriatic tissue more effectively than calcipotriol. In summary, ApoA-I administered from both the apical and basolateral sides exhibits pronounced anti-inflammatory activity in a 3D human psoriasis model by reducing the production of chemokines responsible for immune cell recruitment to sites of inflammation, as well as the expression of psoriasis-associated biomarkers HBD-2 and psoriasin/S100A7. In addition, ApoA-I influences tissue morphology by reducing the thickness of the cornified layer. Collectively, these findings support the further evaluation of ApoA-I as a potential therapeutic approach for psoriatic skin inflammation.

Discussion

Complexes formed by LL-37 and self-nucleic acids have have been implicated in several immune-mediated disorders, including psoriasis[12, 20–22], SLE[12, 13, 19], atherosclerosis[5, 55], and inflammatory myopathies[56]. Their accumulation markedly amplifies inflammatory responses, promoting the breakdown of immune tolerance and the development of autoimmune reactions. Accordingly, multiple therapeutic strategies targeting free nucleic acids have been explored, including scavenging extracellular nucleic acids, inhibiting intracellular nucleic acid-sensing receptors, and enhancing endogenous degradation pathways[57–59]. These approaches have been shown to limit pathological inflammation and nucleic acid-driven autoimmunity[57, 58, 60–62]. However, while such strategies reduce the availability and proinflammatory activity of free nucleic acids, LL-37 remains unbound and may continue to exert deleterious effects. Our findings suggest that ApoA-I may interfere with both LL-37:nucleic acid-dependent immune activation and the direct effects of LL-37. Dissociation of these complexes could also increase the accessibility of released nucleic acids to enzymatic degradation, although this possibility requires further investigation. Collectively, these results support further evaluation of ApoA-I, alone or in combination with nucleic acid-targeting approaches, for limiting LL-37-associated inflammation in psoriasis.

It is important to note that by neutralizing LL-37 activity, ApoA-I may interfere with this pathogenic feed-forward loop at multiple levels. Specifically, ApoA-I reduced neutrophil recruitment and activation and inhibited LL-37-induced NET formation [**Supplementary Fig. 5**], potentially limiting subsequent inflammatory signaling driven by DAMPs released from damaged and dying cells. These findings suggest that ApoA-I could modulate LL-37-dependent inflammation during both the initiation and maintenance phases of psoriasis. They also raise the possibility that targeting LL-37 may be relevant to other neutrophil-driven inflammatory dermatoses, although this potential requires disease-specific investigation.

A growing body of evidence demonstrates that ApoA-I levels are reduced in chronic inflammatory disorders characterized by aberrant innate immune activation and extracellular nucleic acid sensing. This appears particularly relevant in diseases where LL-37:DNA or LL-37:RNA complexes have been implicated in disease pathogenesis. Several studies have reported significantly reduced circulating ApoA-I levels in psoriasis patients, often correlating inversely with disease severity and systemic inflammatory burden. Indeed, a recent meta-analysis by Wang *et al.* including 17 studies and 2467 participants confirmed decreased serum ApoA-I levels in psoriasis compared with healthy controls[63]. Holzer *et al.* further demonstrated reduced ApoA-I content together with impaired anti-inflammatory properties in psoriasis-associated lipoprotein particles[64]. LL-37:self-nucleic acid complexes have also been implicated in SLE, where NETs enriched in LL-37 and self-DNA activate pDCs and promote type I interferon-driven inflammation[13, 65]. Reduced ApoA-I levels have likewise been associated with SLE disease activity and chronic inflammation. SLE patients exhibit significantly reduced ApoA-I levels across age groups, with ApoA-I inversely associated with inflammatory activity and disease severity

measures[66]. Similar mechanisms involving extracellular DNA sensing and neutrophil activation have been discussed in rheumatoid arthritis and related autoimmune inflammatory disorders[67].

Mechanistically, chronic inflammation may reduce ApoA-I availability through oxidative and proteolytic pathways. Neutrophil-rich inflammatory environments contain enzymes capable of modifying or degrading ApoA-I. Shao *et al.* demonstrated that MPO-mediated oxidation of ApoA-I impairs its biological and anti-inflammatory properties[68]. In parallel, inflammatory proteases including cathepsin S and matrix metalloproteinases can degrade ApoA-I[69, 70]. Such mechanisms may be particularly relevant in psoriatic lesions, which are characterized by abundant neutrophils and neutrophil elastase activity[71, 72]. In this context, ApoA-I depletion could diminish an endogenous buffering mechanism limiting LL-37:DNA-mediated immune activation. Thus, reduced ApoA-I levels in psoriasis and related inflammatory diseases may not merely represent a biomarker of inflammation, but potentially contribute directly to amplification of LL-37-driven inflammatory responses.

To date, several ApoA-I-based molecules have been evaluated in clinical trials, including recombinant forms of the protein and reconstituted HDL formulations. ApoA-I protein combined with phospholipids has been tested for the treatment of atherosclerosis (e.g., ETC-216, CSL-111, CSL-112)[73–75]. Although these formulations showed a trend toward reducing atherosclerotic plaque volume, their clinical utility was limited by hepatotoxic effects. While our studies did not reveal harmful systemic effects of ApoA-I, we further demonstrate that intradermal delivery achieves comparable therapeutic efficacy while substantially reducing the risk of off-target organ toxicity. Beyond the native protein, ApoA-I mimetic peptides, including L-4F, D-4F, and ETC-642, have been developed to reproduce the amphipathic α-helical structure central to ApoA-I function[76–78]. These peptides bind cholesterol and fatty acids and exert potent anti-inflammatory effects, recapitulating key aspects of ApoA-I activity in a simplified molecular format. Although ApoA-I mimetic peptides represent a cost-effective alternative to the full-length protein, their clinical translation has been limited by inefficient delivery to sites of action, poor oral bioavailability, and modest efficacy observed in clinical trials. While we did not evaluate ApoA-I-derived peptides, our interaction studies identify regions of ApoA-I that may contribute to LL-37 binding. These observations provide a basis for future studies examining whether shorter ApoA-I-derived fragments can retain LL-37-binding and neutralizing activity. Local delivery of either ApoA-I or such derivatives could potentially increase exposure at the site of inflammation while limiting systemic exposure, but this possibility requires further pharmacokinetic, efficacy, and safety evaluation.

In summary, our findings demonstrate that ApoA-I exerts a regulatory effect on inflammatory processes by neutralizing the proinflammatory activity of LL-37 complexed with nucleic acids-key drivers of the exaggerated immune responses characteristic of psoriasis. By integrating a comprehensive experimental strategy encompassing in vitro SALT-cell models, the IMQ-induced murine psoriasis model, and a 3D human psoriatic skin tissue model, we identified a previously unrecognized therapeutic role for ApoA-I. Collectively, these data support further investigation of ApoA-I as a potential therapeutic approach for LL-37-associated inflammation in psoriasis.

Declarations

Author contributions:

Conceptualization: JK. Methodology: AG, MRK. Investigation: AG, AW, DK, KA, DB, DS, FS, PJB. Resources: JP. Visualization: AG, JK, DB. Supervision: JK. Writing-original draft: AG, JK. Writing-review and editing: AG, AS, JP, JK.

Acknowledgements:

This project has been supported by Centre for Technology Transfer CITTRU, Jagiellonian University, grant *Białko osocza ludzkiego w walce z łuszczycą, IDUJ*. We acknowledge Proteomics Core Facility of the Faculty of Biochemistry, Biophysics and Biotechnology and the Malopolska Centre of Biotechnology at the Jagiellonian University for mass spectrometry analysis. The purchase of Orbitrap Astral Mass Spectrometer has been supported by a grant from the Priority Research Area (POB BioS) under the Strategic Programme Excellence Initiative at Jagiellonian University. Simulations were performed on resources of the National Supercomputing Centre, Singapore (https://www.nscc.sg) and the A*STAR Computational Resource Centre (A*CRC). P. J. B. and F. S. are supported by BII (A*STAR) core funds.

Data availability:

The datasets generated and/or analyzed during the current study will be deposited in the Jagiellonian University collection of RODBUK (Cracow Open Research Data Repository) upon acceptance of the manuscript for publication. The accession number and DOI will be provided upon data deposition

References

1. Oren Z, Lerman JC, Gudmundsson GH, Agerberth B, Shai Y (1999) Structure and organization of the human antimicrobial peptide LL-37 in phospholipid membranes: relevance to the molecular basis for its non-cell-selective activity. Biochem J 341(Pt 3):501–513
2. Travis SM, Anderson NN, Forsyth WR et al (2000) Bactericidal activity of mammalian cathelicidin-derived peptides. Infect Immun 68:2748–2755
3. Nagaoka I, Hirota S, Niyonsaba F et al (2002) Augmentation of the lipopolysaccharide-neutralizing activities of human cathelicidin CAP18/LL-37-derived antimicrobial peptides by replacement with hydrophobic and cationic amino acid residues. Clin Diagn Lab Immunol 9:972–982
4. Sall J, Carlsson M, Gidlof O et al (2013) The antimicrobial peptide LL-37 alters human osteoblast Ca2 + handling and induces Ca2+-independent apoptosis. J Innate Immun 5:290–300
5. Ciornei CD, Tapper H, Bjartell A, Sternby NH, Bodelsson M (2006) Human antimicrobial peptide LL-37 is present in atherosclerotic plaques and induces death of vascular smooth muscle cells: a

laboratory study. BMC Cardiovasc Disord 6:49

6. Jonsson D, Nilsson BO (2012) The antimicrobial peptide LL-37 is anti-inflammatory and proapoptotic in human periodontal ligament cells. J Periodontal Res 47:330–335
7. Mader JS, Ewen C, Hancock RE, Bleackley RC (2011) The human cathelicidin, LL-37, induces granzyme-mediated apoptosis in regulatory T cells. J Immunother 34:229–235
8. Zhang Z, Cherryholmes G, Shively JE (2008) Neutrophil secondary necrosis is induced by LL-37 derived from cathelicidin. J Leukoc Biol 84:780–788
9. Nagaoka I, Tamura H, Reich J (2020) Therapeutic Potential of Cathelicidin Peptide LL-37, an Antimicrobial Agent, in a Murine Sepsis Model. Int J Mol Sci ;21
10. Tjabringa GS, Ninaber DK, Drijfhout JW, Rabe KF, Hiemstra PS (2006) Human cathelicidin LL-37 is a chemoattractant for eosinophils and neutrophils that acts via formyl-peptide receptors. Int Arch Allergy Immunol 140:103–112
11. De Y, Chen Q, Schmidt AP et al (2000) LL-37, the neutrophil granule- and epithelial cell-derived cathelicidin, utilizes formyl peptide receptor-like 1 (FPRL1) as a receptor to chemoattract human peripheral blood neutrophils, monocytes, and T cells. J Exp Med 192:1069–1074
12. Gilliet M, Cao W, Liu YJ (2008) Plasmacytoid dendritic cells: sensing nucleic acids in viral infection and autoimmune diseases. Nat Rev Immunol 8:594–606
13. Lande R, Ganguly D, Facchinetti V et al (2011) Neutrophils activate plasmacytoid dendritic cells by releasing self-DNA-peptide complexes in systemic lupus erythematosus. Sci Transl Med 3:73ra19
14. Alford MA, Baquir B, Santana FL, Haney EF, Hancock REW (2020) Cathelicidin Host Defense Peptides and Inflammatory Signaling: Striking a Balance. Front Microbiol 11:1902
15. Kahlenberg JM, Kaplan MJ (2013) Little peptide, big effects: the role of LL-37 in inflammation and autoimmune disease. J Immunol 191:4895–4901
16. Hoffmann MH, Bruns H, Backdahl L et al (2013) The cathelicidins LL-37 and rCRAMP are associated with pathogenic events of arthritis in humans and rats. Ann Rheum Dis 72:1239–1248
17. Zhang J, Xu X, Rao NV et al (2011) Novel sulfated polysaccharides disrupt cathelicidins, inhibit RAGE and reduce cutaneous inflammation in a mouse model of rosacea. PLoS ONE 6:e16658
18. Yamasaki K, Di Nardo A, Bardan A et al (2007) Increased serine protease activity and cathelicidin promotes skin inflammation in rosacea. Nat Med 13:975–980
19. Kahlenberg JM, Carmona-Rivera C, Smith CK, Kaplan MJ (2013) Neutrophil extracellular trap-associated protein activation of the NLRP3 inflammasome is enhanced in lupus macrophages. J Immunol 190:1217–1226
20. Lande R, Gregorio J, Facchinetti V et al (2007) Plasmacytoid dendritic cells sense self-DNA coupled with antimicrobial peptide. Nature 449:564–569
21. Ganguly D, Chamilos G, Lande R et al (2009) Self-RNA-antimicrobial peptide complexes activate human dendritic cells through TLR7 and TLR8. J Exp Med 206:1983–1994

22. Zhang LJ, Sen GL, Ward NL et al (2016) Antimicrobial Peptide LL37 and MAVS Signaling Drive Interferon-beta Production by Epidermal Keratinocytes during Skin Injury. Immunity 45:119–130
23. WHO (2016) Global report on psoriasis. Geneva: World Health Organ
24. Boehncke WH, Schon MP, Psoriasis (2015) Lancet 386:983–994
25. Griffiths CE, Barker JN (2007) Pathogenesis and clinical features of psoriasis. Lancet 370:263–271
26. Nestle FO, Kaplan DH, Barker J, Psoriasis (2009) N Engl J Med 361:496–509
27. Lowes MA, Bowcock AM, Krueger JG (2007) Pathogenesis and therapy of psoriasis. Nature 445:866–873
28. Griffiths CEM, Armstrong AW, Gudjonsson JE, Barker J, Psoriasis (2021) Lancet 397:1301–1315
29. Bergsson G, Reeves EP, McNally P et al (2009) LL-37 complexation with glycosaminoglycans in cystic fibrosis lungs inhibits antimicrobial activity, which can be restored by hypertonic saline. J Immunol 183:543–551
30. Wong A, Bryzek D, Dobosz E et al (2018) A Novel Biological Role for Peptidyl-Arginine Deiminases: Citrullination of Cathelicidin LL-37 Controls the Immunostimulatory Potential of Cell-Free DNA. J Immunol 200:2327–2340
31. Yoshida K, Suzuki S, Kawada-Matsuo M et al (2019) Heparin-LL37 complexes are less cytotoxic for human dental pulp cells and have undiminished antimicrobial and LPS-neutralizing abilities. Int Endod J 52:1327–1343
32. Queme-Pena M, Ricci M, Juhasz T et al (2021) Old Polyanionic Drug Suramin Suppresses Detrimental Cytotoxicity of the Host Defense Peptide LL-37. ACS Pharmacol Transl Sci 4:155–167
33. Rye KA, Bursill CA, Lambert G, Tabet F, Barter PJ (2009) The metabolism and anti-atherogenic properties of HDL. J Lipid Res 50(Suppl):S195–200
34. Wang Y, Agerberth B, Lothgren A, Almstedt A, Johansson J (1998) Apolipoprotein A-I binds and inhibits the human antibacterial/cytotoxic peptide LL-37. J Biol Chem 273:33115–33118
35. Koziel J, Bryzek D, Sroka A et al (2014) Citrullination alters immunomodulatory function of LL-37 essential for prevention of endotoxin-induced sepsis. J Immunol 192:5363–5372
36. Kozakov D, Hall DR, Xia B et al (2017) The ClusPro web server for protein-protein docking. Nat Protoc 12:255–278
37. Borhani DW, Rogers DP, Engler JA, Brouillette CG (1997) Crystal structure of truncated human apolipoprotein A-I suggests a lipid-bound conformation. Proc Natl Acad Sci U S A 94:12291–12296
38. Jumper J, Evans R, Pritzel A et al (2021) Highly accurate protein structure prediction with AlphaFold. Nature 596:583–589
39. Huang J, MacKerell AD Jr. (2013) CHARMM36 all-atom additive protein force field: validation based on comparison to NMR data. J Comput Chem 34:2135–2145
40. Hoover WG (1985) Canonical dynamics: Equilibrium phase-space distributions. Phys Rev Gen Phys 31:1695–1697

41. Nosé S (1984) A unified formulation of the constant temperature molecular dynamics methods. J Chem Phys 81:511–519
42. Parrinello M, Rahman A (1981) Polymorphic transitions in single crystals: A new molecular dynamics method. J Appl Phys 52:7182–7190
43. Essmann U, Perera L, Berkowitz ML, Darden T, Lee H, Pedersen LG (1995) A smooth particle mesh Ewald method. J Chem Phys 103:8577–8593
44. Hess B, Bekker H, Berendsen HJC, Fraaije JGEM (1997) LINCS: A linear constraint solver for molecular simulations. J Comput Chem 18:1463–1472
45. Abraham MJ, Murtola TJ, Schulz R et al (2015) GROMACS: High performance molecular simulations through multi-level parallelism from laptops to supercomputers. SoftwareX 1–2:19–25
46. Humphrey W, Dalke A, Schulten K (1996) VMD: visual molecular dynamics. J Mol Graph 14:33–38
47. Bryzek D, Golda A, Budziaszek J et al (2020) Citrullination-Resistant LL-37 Is a Potent Antimicrobial Agent in the Inflammatory Environment High in Arginine Deiminase Activity. Int J Mol Sci ;21
48. van der Fits L, Mourits S, Voerman JS et al (2009) Imiquimod-induced psoriasis-like skin inflammation in mice is mediated via the IL-23/IL-17 axis. J Immunol 182:5836–5845
49. Livak KJ, Schmittgen TD (2001) Analysis of relative gene expression data using real-time quantitative PCR and the 2(-Delta Delta C(T)) Method. Methods 25:402–408
50. Hughes CS, Moggridge S, Muller T, Sorensen PH, Morin GB, Krijgsveld J (2019) Single-pot, solid-phase-enhanced sample preparation for proteomics experiments. Nat Protoc 14:68–85
51. Demichev V, Messner CB, Vernardis SI, Lilley KS, Ralser M (2020) DIA-NN: neural networks and interference correction enable deep proteome coverage in high throughput. Nat Methods 17:41–44
52. Tyanova S, Temu T, Sinitcyn P et al (2016) The Perseus computational platform for comprehensive analysis of (prote)omics data. Nat Methods 13:731–740
53. Nestle FO, Di Meglio P, Qin JZ, Nickoloff BJ (2009) Skin immune sentinels in health and disease. Nat Rev Immunol 9:679–691
54. Girolomoni G, Strohal R, Puig L et al (2017) The role of IL-23 and the IL-23/T(H) 17 immune axis in the pathogenesis and treatment of psoriasis. J Eur Acad Dermatol Venereol 31:1616–1626
55. Doring Y, Manthey HD, Drechsler M et al (2012) Auto-antigenic protein-DNA complexes stimulate plasmacytoid dendritic cells to promote atherosclerosis. Circulation 125:1673–1683
56. Lu X, Tang Q, Lindh M et al (2017) The host defense peptide LL-37 a possible inducer of the type I interferon system in patients with polymyositis and dermatomyositis. J Autoimmun 78:46–56
57. Lee J, Sohn JW, Zhang Y, Leong KW, Pisetsky D, Sullenger BA (2011) Nucleic acid-binding polymers as anti-inflammatory agents. Proc Natl Acad Sci U S A 108:14055–14060
58. Holl EK, Shumansky KL, Borst LB et al (2016) Scavenging nucleic acid debris to combat autoimmunity and infectious disease. Proc Natl Acad Sci U S A 113:9728–9733
59. Zhao L, Liang K, Cheng W et al (2025) A multifaceted strategy for intra- and extracellular nucleic acid regulation to alleviate intervertebral disc degeneration. Nat Commun 16:7936

60. Liang H, Yan Y, Wu J et al (2020) Topical nanoparticles interfering with the DNA-LL37 complex to alleviate psoriatic inflammation in mice and monkeys. Sci Adv 6:eabb5274
61. Huang H, Pan W, Wang Y et al (2022) Nanoparticulate cell-free DNA scavenger for treating inflammatory bone loss in periodontitis. Nat Commun 13:5925
62. Liang H, Peng B, Dong C et al (2018) Cationic nanoparticle as an inhibitor of cell-free DNA-induced inflammation. Nat Commun 9:4291
63. Wang F, Wang Y, Kong X et al (2023) Association between psoriasis and serum apolipoprotein A1 and B: A systematic review and meta-analysis. Heliyon 9:e21168
64. Holzer M, Wolf P, Curcic S et al (2012) Psoriasis alters HDL composition and cholesterol efflux capacity. J Lipid Res 53:1618–1624
65. Garcia-Romo GS, Caielli S, Vega B et al (2011) Netting neutrophils are major inducers of type I IFN production in pediatric systemic lupus erythematosus. Sci Transl Med 3:73ra20
66. Jury EC, Peng J, Van Vijfeijken A et al (2024) Systemic lupus erythematosus patients have unique changes in serum metabolic profiles across age associated with cardiometabolic risk. Rheumatology (Oxford) 63:2741–2753
67. Lei J, Liu M, Huang X, Zhai X, Ji H, Wen Z (2025) The Immunogenic Role of Self-DNA in T Cell Immunity. Clin Rev Allergy Immunol 68:101
68. Shao B, Oda MN, Oram JF, Heinecke JW (2006) Myeloperoxidase: an inflammatory enzyme for generating dysfunctional high density lipoprotein. Curr Opin Cardiol 21:322–328
69. Gebhard C, Maafi F, Stahli BE et al (2018) Apolipoprotein A-I proteolysis in aortic valve stenosis: role of cathepsin S. Basic Res Cardiol 113:30
70. Salminen A, Astrom P, Metso J et al (2015) Matrix metalloproteinase 8 degrades apolipoprotein A-I and reduces its cholesterol efflux capacity. FASEB J 29:1435–1445
71. Wiedow O, Wiese F, Christophers E (1995) Lesional elastase activity in psoriasis. Diagnostic and prognostic significance. Arch Dermatol Res 287:632–635
72. Wiedow O, Wiese F, Streit V, Kalm C, Christophers E (1992) Lesional elastase activity in psoriasis, contact dermatitis, and atopic dermatitis. J Invest Dermatol 99:306–309
73. Nissen SE, Tsunoda T, Tuzcu EM et al (2003) Effect of recombinant ApoA-I Milano on coronary atherosclerosis in patients with acute coronary syndromes: a randomized controlled trial. JAMA 290:2292–2300
74. Tardif JC, Gregoire J, L'Allier PL et al (2007) Effects of reconstituted high-density lipoprotein infusions on coronary atherosclerosis: a randomized controlled trial. JAMA 297:1675–1682
75. Gibson CM, Duffy D, Bahit MC et al (2024) Apolipoprotein A-I infusions and cardiovascular outcomes in acute myocardial infarction according to baseline LDL-cholesterol levels: the AEGIS-II trial. Eur Heart J 45:5023–5038
76. Bloedon LT, Dunbar R, Duffy D et al (2008) Safety, pharmacokinetics, and pharmacodynamics of oral apoA-I mimetic peptide D-4F in high-risk cardiovascular patients. J Lipid Res 49:1344–1352

77. Watson CE, Weissbach N, Kjems L et al (2011) Treatment of patients with cardiovascular disease with L-4F, an apo-A1 mimetic, did not improve select biomarkers of HDL function. J Lipid Res 52:361–373
78. Navab M, Anantharamaiah GM, Hama S et al (2002) Oral administration of an Apo A-I mimetic Peptide synthesized from D-amino acids dramatically reduces atherosclerosis in mice independent of plasma cholesterol. Circulation 105:290–292

Figures

Figure 1

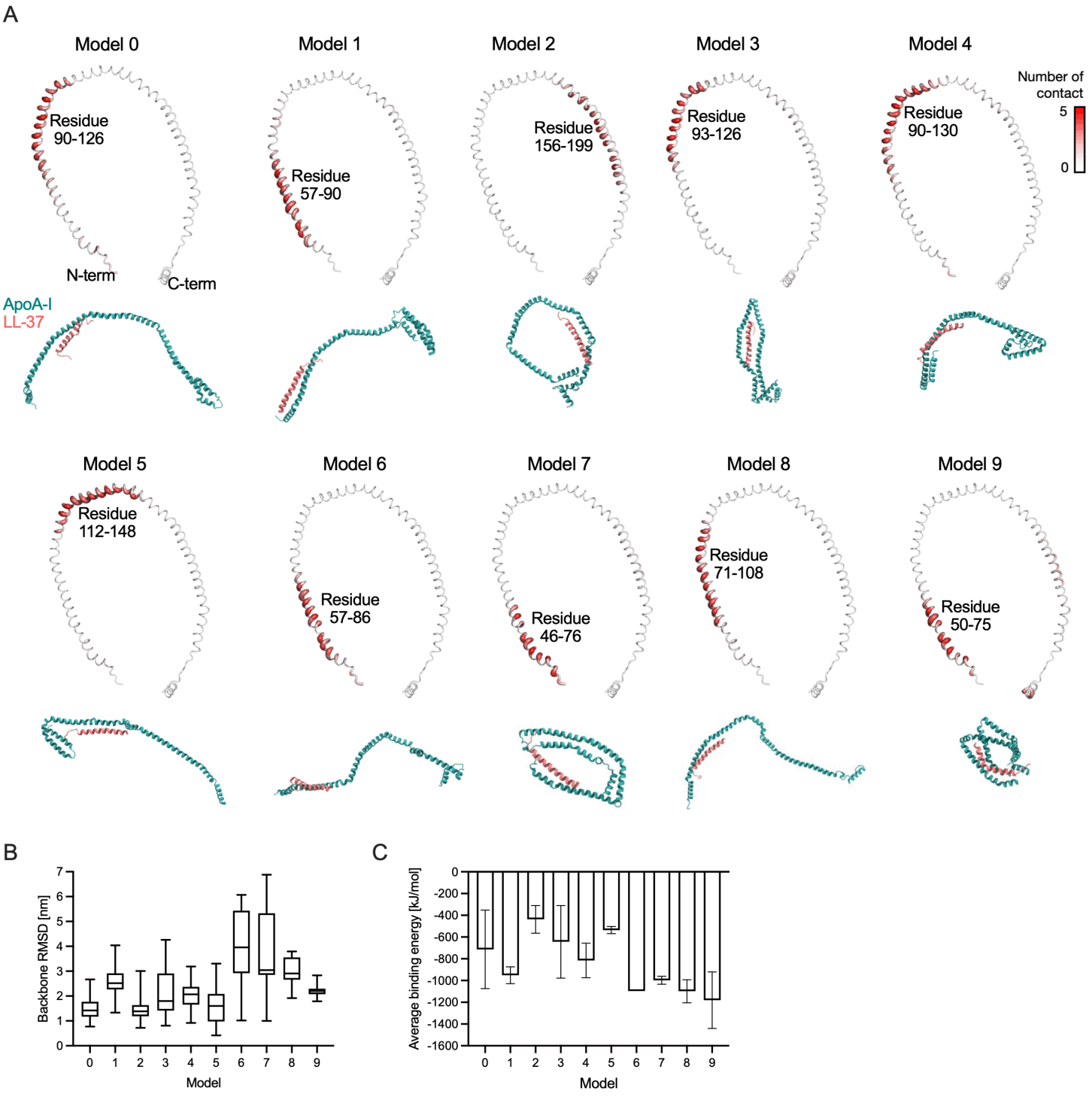


Figure 1

Heterogeneous binding of LL-37 to ApoA-I with N-terminal preference. (A) (Top) Average number of contacts made by LL-37 peptide with ApoA-I from 3 × 200 ns atomistic MD simulations, mapped to the structure of ApoA-I monomer. The residue ranges with the highest number of contacts are labelled. (Bottom) The final snapshots from one of the simulations with ApoA-I shown in cyan and the LL-37 peptide shown in pink. (B) Distribution of RMSD of the backbone atoms of the LL-37 peptide after least-

square fitting to the initial structure of the ApoA-I:LL37 protein complex. The data shown are taken from the last 100 ns of the three independent simulations. (C) Mean MM/PBSA binding free energy calculated over the final 100 ns of the three independent simulations. Standard deviations are depicted as the error bars.

Figure 2

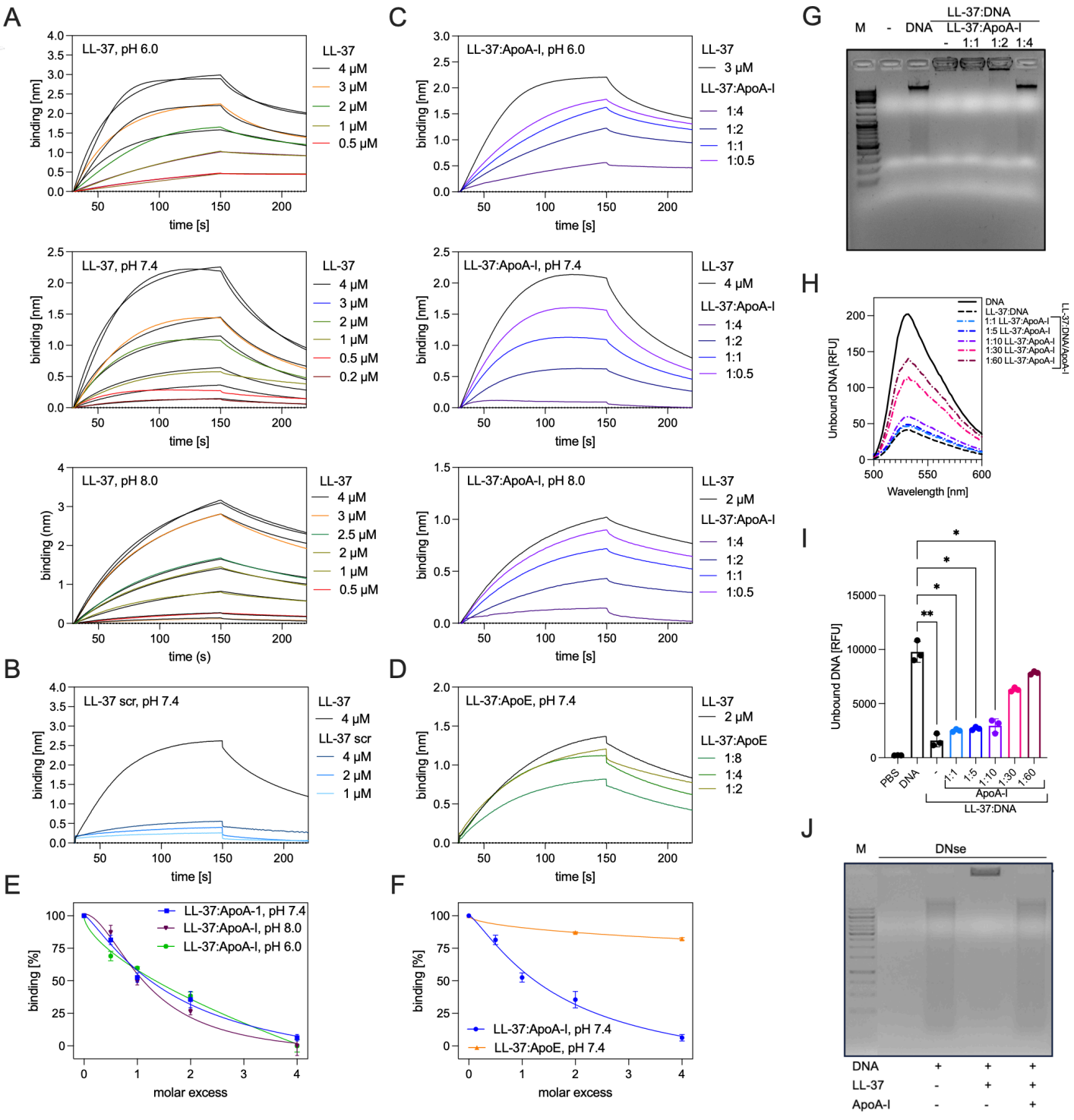


Figure 2

***LL-37 complexed with ApoA-I does not interact with nucleic acids, while ApoA-I promotes dissociation of LL-37:nucleic acid complexes*.** (A) Bio-layer interferometry (BLI) analysis of LL-37 binding to DNA. Sensorgrams were recorded by dipping a SAX biosensor with immobilized DNA into LL-37 solutions at increasing concentrations at different pH values. Black lines show fits to a Langmuir 1:1 binding model. (B) Scrambled LL-37 (LL-37 scr), with identical amino acid composition but a randomized sequence, served as a control for non-specific interactions. (C) LL-37 was preincubated with ApoA-I before exposure to immobilized DNA. ApoA-I was used at molar ratios of 0.5-4 to LL-37 at pH 6.0, 7.4, and 8.0. (D) Apolipoprotein E (ApoE) served as a control for interaction specificity. (E) Binding analysis of LL-37 to DNA in the presence of ApoA-I (*n* = 2; mean ± SD). (F) Comparison of LL-37 binding to DNA in the presence of ApoA-I and control ApoE (*n* = 2; mean ± SD). (G) Classical electrophoretic shift assay (EMSA) revealed that addition of ApoA-I to the LL-37:DNA complex results in the release of DNA from the complex with LL-37. (H, I). The dissociation of DNA from LL-37:nucleic acid complex in the presence of ApoA-I was further confirmed by spectral analysis. Unbound DNA was quantified with spectral analysis using PicoGreen and is shown as relative fluorescence units (RFU) (*n*= 3; mean ± SD). (J) Electrophoretic analysis of LL-37:DNA complexes and complexes treated with ApoA-I followed by nuclease exposure. Nucleic acids released from LL-37 complexes were degraded by nucleases. Statistical significance was evaluated by one-way ANOVA followed by Šídák's multiple comparisons test (*p < 0.05; **p < 0.01).

Figure 3

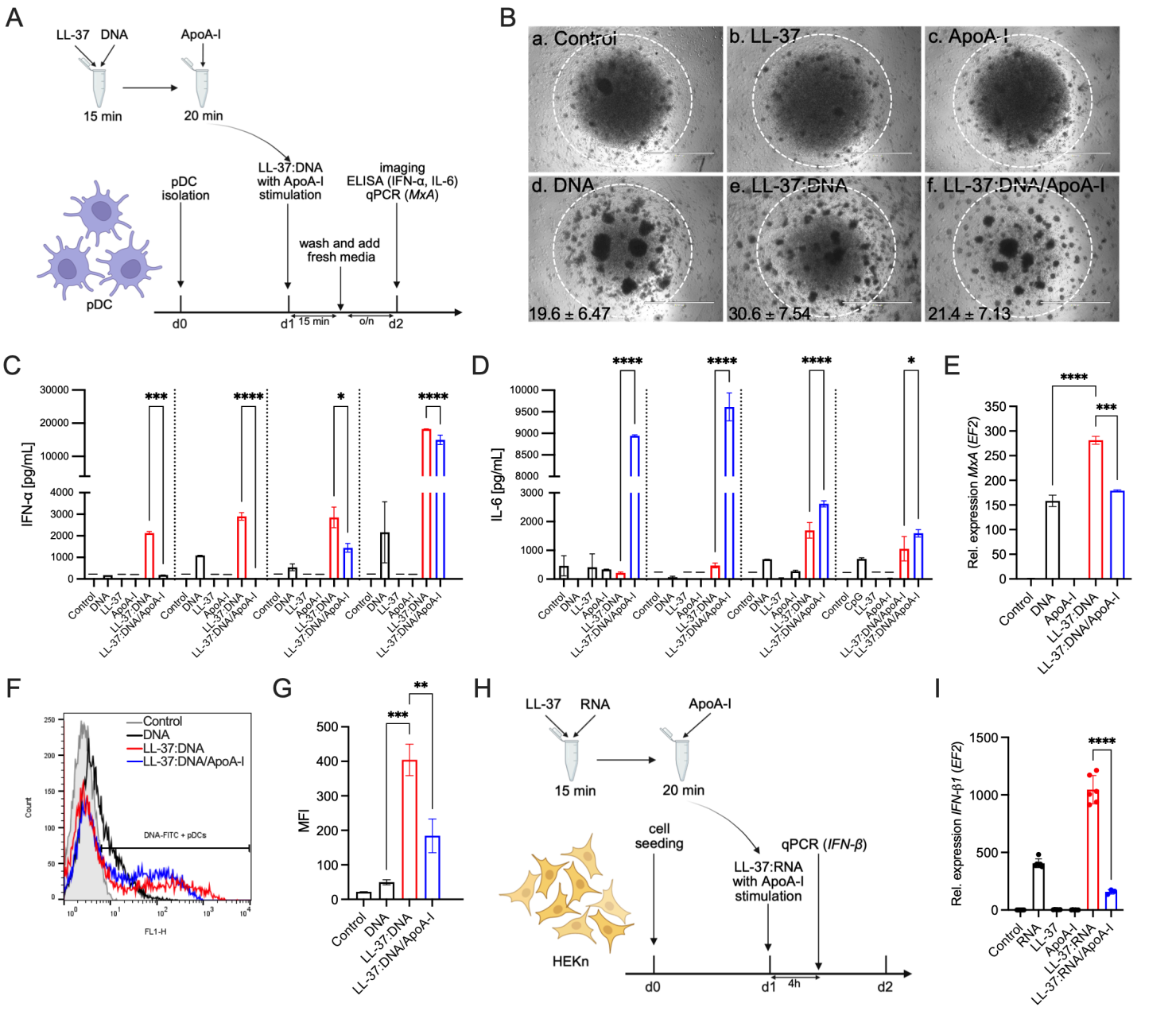


Figure 3

ApoA-I efficiently prevents inflammation induced by LL-37:nucleic acids complexes. (A) Schematic overview of the experimental setup for the pDCs experiments. (B) Formation of cell clumps reflecting the activation of human pDCs. Number of cell clumps counts is shown in the lower left corner of the images. (C, D) ApoA-I down-regulates IFN-α and up-regulates IL-6 induced by the LL-37:DNA complex in human pDCs. IFN-α and IL-6 production in the cell culture supernatant was measured with ELISA (*n* = 4; mean ± SD). Hyphens indicate values below the limit of detection (not detected). (E) *MxA* mRNA expression confirmed IFN-α protein results (mean ± SD). Representative data from one of three independent donors are shown. (F, G) Flow cytometry analysis of pDCs to assess uptake of DNA alone, DNA complexed with LL-37 and LL-37:DNA complexes in the presence of ApoA-I (mean ± SD). Representative data from one

of three independent donors are shown. (H) Schematic overview of the experimental setup for the HEKn experiments. (I) ApoA-I inhibits IFN-β expression in primary human keratinocytes (n = 3; mean ± SD). Statistical significance was evaluated by one-way ANOVA followed by Šídák's multiple comparisons test (*p < 0.05; **p < 0.01; ***p < 0.01; ****p < 0.0001).

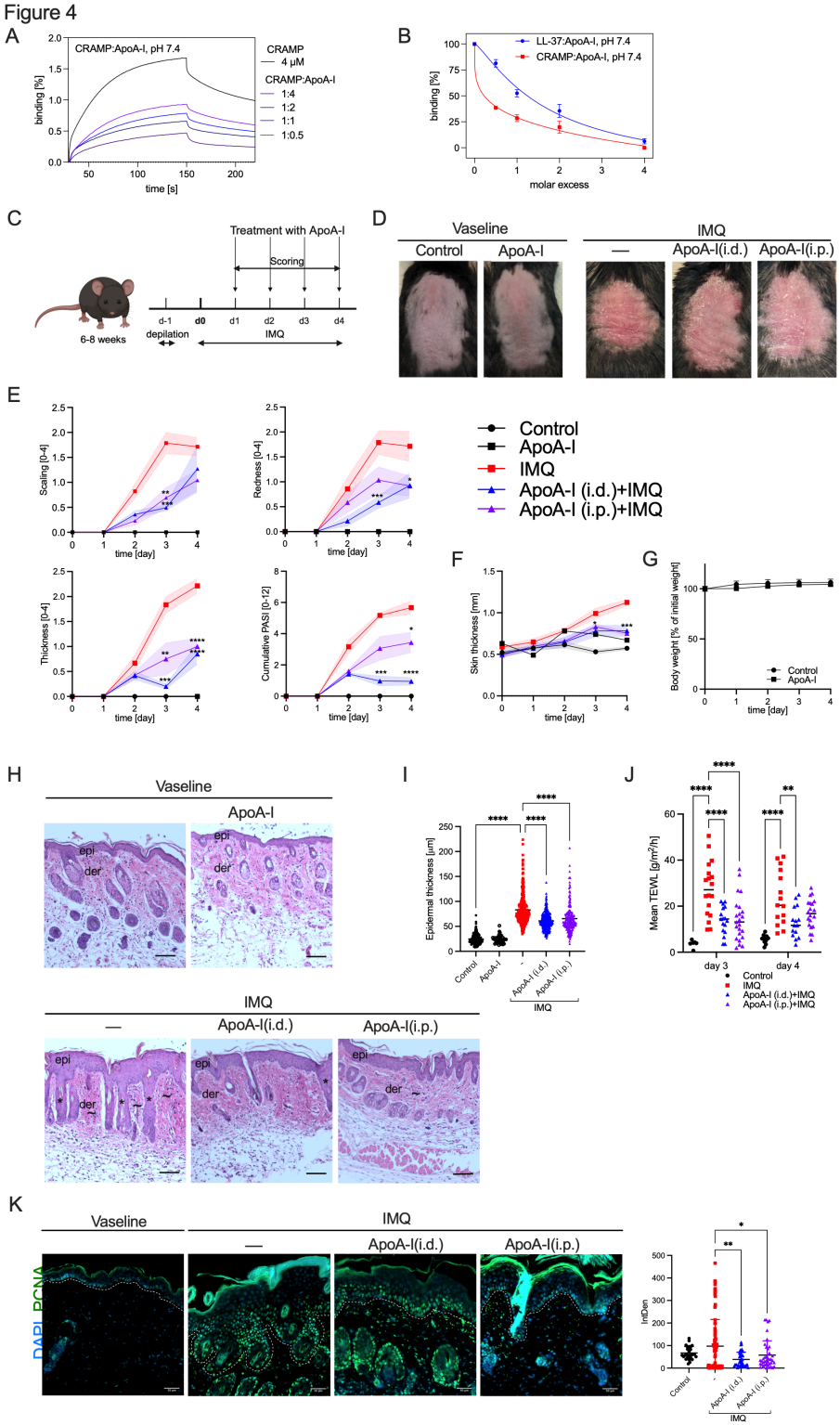


Figure 4

ApoA-I treatment ameliorates psoriasiform skin inflammation of IMQ mice. (A) Bio-layer interferometry (BLI) analysis of CRAMP binding to DNA. CRAMP was preincubated with ApoA-I before exposure to immobilized DNA. ApoA-I was used at a 0.5–4 fold molar excess relative to CRAMP at pH 7.4. (B) Comparison of LL-37 or CRAMP binding to DNA in the presence of ApoA-I (*n* = 2; mean ± SD). (C) Schematic overview of the experimental setup for the in vivo experiments. Acute psoriasis-like skin inflammation developed after daily application of IMQ cream on back skin for 5 days (d0 – d4). Starting from day 1 (d1) ApoA-I was applied daily (i.d. or i.p.) at a dose of 800 μg/mL. Further analysis was performed after sacrificing the mice at day 4. (D) Representative skin surface morphology of the dorsal skin from all mouse groups: control, ApoA-I treated, IMQ treated, and IMQ with ApoA-I treated mice. (E) Scaling, erythema, and thickness of the back skin were scored daily from 0 to 4. Additionally, the cumulative score as the sum of scaling, erythema, and thickness scores is presented (*n* > 4; mean ± SD). (F) Dorsal skin thickness in mice was measured daily throughout the experiment (*n* > 4; mean ± SD). (G) Additionally, animal body weight was monitored throughout the experiment (*n* > 4; mean ± SEM). (H) Representative hematoxylin and eosin (H&E) staining of skin sections from all groups at day 4. Elongated epidermal rete ridges (asterisks) and infiltration of inflammatory cells (tilde) within dermis were evidently visible in IMQ treated mice. Scale bar: 50 μm. (I) Analysis of the thickness of the epidermal layer of mouse back skin in H&E stained sections by ImageJ software. (J) Transepidermal Water Loss (TEWL) was measured (*n* > 4; mean ± SD). (K) Representative immunohistochemical images and quantification of PCNA expression (green) in skin sections from the various mice groups at day 4. Cell nuclei were stained with DAPI (blue). Location of the basal membrane is indicated with a white dotted line. Scale bar: 50 μm. Analysis of the PCNA expression in epidermis of mouse back skin by ImageJ software. Statistical significance was evaluated by one-way ANOVA or two-way ANOVA followed by Šídák's multiple comparisons test (*p < 0.05; **p < 0.01; ***p < 0.001; ****p < 0.0001).

Figure 5

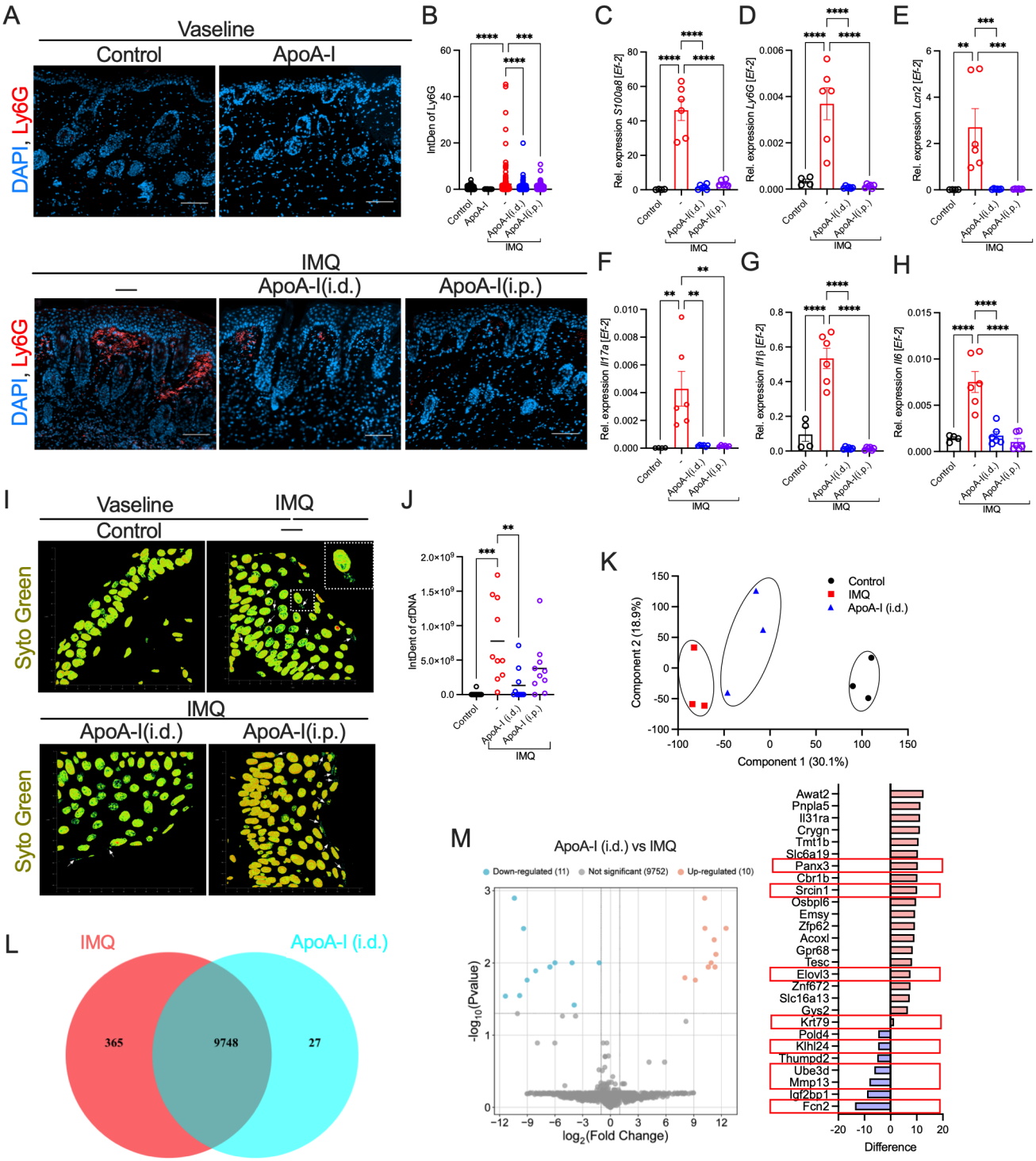


Figure 5

ApoA-I reduces proinflammatory cytokine expression and neutrophil infiltration. (A) Immunofluorescence detection of neutrophils (Ly6G$^+$, red) in the psoriatic skin of all mouse groups: control, ApoA-I treated, IMQ treated, and IMQ with ApoA-I treated mice. Cell nuclei were stained with DAPI (blue). Scale bar: 50 μm. (B) Red fluorescence was quantified using ImageJ software and is presented as mean ± SEM. (C, D, E) mRNA levels of neutrophil marker transcripts including *S100a8*, *Ly6G* and *Lcn2* (control *n* = 4; IMQ,

IMQ+ApoA-I (i.d.), IMQ+ApoA-I (i.p.) *n* = 6; mean ± SEM). (F, G, H) mRNA levels of proinflammatory cytokines involved in psoriasis pathogenesis *Il-17a*, *Il-1β*, and *Il-6* in skin at day 4 (control *n* = 4; IMQ, IMQ+ApoA-I (i.d.), IMQ+ApoA-I (i.p.) *n* = 6; mean ± SEM). (I) Confocal images of cfDNA in the psoriatic skin stained with SYTOX Green. Arrows indicate cfDNA. Additionally, enlarged image fragment is shown to better illustrate the distinct structure of cfDNA. Scale bar: 50 μm. (J) The fluorescence between cell nuclei was quantified using ImageJ software and is presented as mean. (K) Principal component analysis (PCA) showing differences between the three analyzed groups of proteomes (control, IMQ, ApoA-I i.d.). (L) Venn diagram presenting all identified proteins in IMQ treated mice and after ApoA-I i.d. stimulation (q-value < 0.05, Benjamini-Hochberg FDR 0.05). (M) Volcano plot of differently abundant protein after ApoA-I i.d. stimulation. The graph shows downregulated and upregulated proteins in the group of mice treated with IMQ and ApoA-I (i.d.). Additionally, proteins that may play a role in the pathogenesis of psoriasis are highlighted with red boxes. Statistical significance was evaluated by one-way ANOVA followed by Šídák's multiple comparisons test (**p < 0.01; ***p < 0.001; ****p < 0.0001).

Figure 6

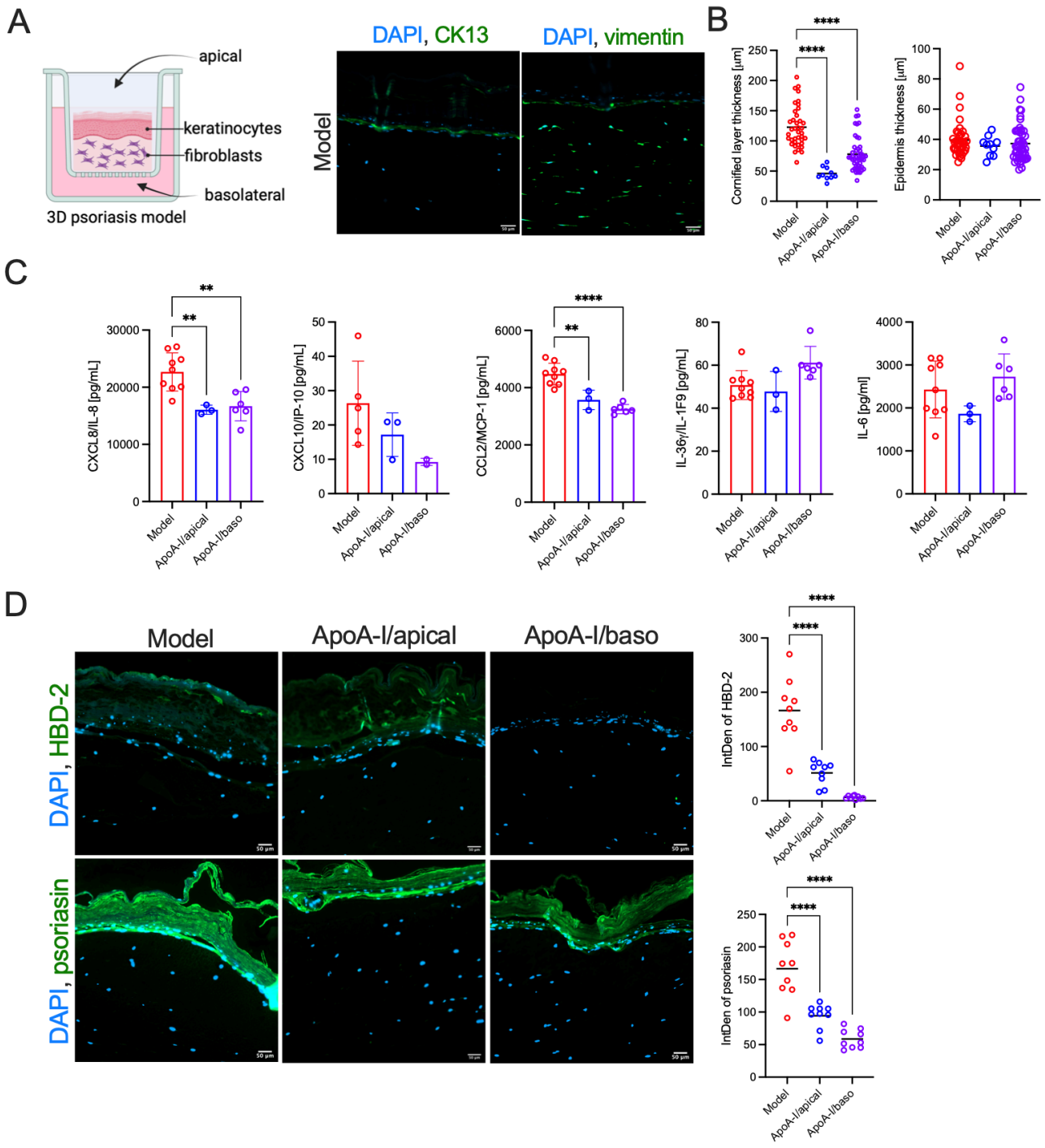


Figure 6

ApoA-I ameliorates psoriasiform features in a 3D human skin model. (A) Schematic representation of the 3D psoriasis tissue model and immunofluorescence detection of cytokeratin 13 and vimentin which confirms the presence of keratinocytes and fibroblasts in 3D psoriasis tissue model. (B) Analysis of cornified layer and epidermis thickness of 3D psoriasis tissue model using ImageJ software and are presented as mean. (C) Inflammatory chemokines and cytokines were assayed with a cytokine bead

array (CBA) kit. The conditioned media of 3D psoriasis tissue model were quantified after being treated with ApoA-I from the apical or basolateral side of insert (model *n* = 9; apical, *n* = 3; basolateral, *n* = 6; mean ± SD). (D) Immunofluorescence detection of psoriasis biomarkers, including human β-defensin-2 (HBD-2), psoriasin/S100A7 (green). Cell nuclei were stained with DAPI (blue). Scale bar: 50 μm. Green fluorescence was quantified using ImageJ software and is presented as mean ± SEM. Statistical significance was evaluated by one-way ANOVA followed by Šídák's multiple comparisons test (**p < 0.01; ****p < 0.0001).

Supplementary Files

This is a list of supplementary files associated with this preprint. Click to download.

- GoldaSupplementaryinformation.pdf